DR 30398
Issue 1

DATE OF PUBLICATION February, 2005

Utilisation of Pulsed Lasers for SEE Testing (Phase 2)

ESTEC Contract No. 16916/02/NL/PA

MBDA
MISSILE SYSTEMS

TITLE	**Utilisation of Pulsed Lasers for SEE Testing (Phase 2)**
	European Space Agency Contract Report
	The work described in this report was performed under ESA Contract No. 16916/02/NL/PA
	Responsibility for the content resides with the author or organisation that prepared it.
	ESA Report Reference ESA_QCA0501S_C
PREPARED & APPOVED ON BEHALF OF MBDA BY	Andrew Chugg Technical Expert, Radiation Physics Radiation Effects Group
AUTHORISED	Rodri Jones Radiation Effects Group Leader
ESTEC TECHNICAL OFFICER	Reno Harboe Sørensen

THIS PAGE INTENTIONALLY LEFT BLANK

CHANGE RECORD SHEET

Issue No.	Date	Page/Paragraphs affected/Summary of Change
1	16/2/05	Initial Issue

THIS PAGE INTENTIONALLY LEFT BLANK

CONTENTS

THIS PAGE INTENTIONALLY LEFT BLANK

ABBREVIATIONS AND GLOSSARY

BICMOS	Bipolar Complementary Metal Oxide Silicon chip technology
CCD	Charge Coupled Device
CCE	Charge Collection Efficiency
COTS	Commercial Off The Shelf
CYCLONE	CYClotron de LOuvaine la NEuve
ESA	European Space Agency
FPGA	Field-Programmable Gate Array
IC	Integrated Circuit
IEEE	Institute of Electrical and Electronics Engineers
LET	Linear Energy Transfer
LINAC	Linear Accelerator
MBU	Multiple Bit Upset
NSREC	Nuclear and Space Radiation Effects Conference
PC	Personal Computer
PWM	Pulse Width Modulator
RADECS	Radiation Effects on Components and Systems
REG	Radiation Effects Group
SEE	Single Event Effect
SEL	Single Event Latchup
SEREEL	Single Event Radiation Effects in Electronics Laser
SET	Single Event Transient
SEU	Single Event Upset
SRAM	Static Random Access Memory
UK	United Kingdom of Great Britain and Northern Ireland

THIS PAGE INTENTIONALLY LEFT BLANK

1 INTRODUCTION AND OVERVIEW

1.1 Phase 2 of the Study

1.1.1 This document constitutes the MBDA Final Report for the European Space Agency's research project on Utilisation of Pulsed Lasers for SEE Testing (Phase 2). This work has been performed under ESA Contract No. 16916/02/NL/PA by the Radiation Effects Group of MBDA UK Limited at Filton in Bristol, England. The work reported here extends and deepens the work performed for Phase 1 of the study under ESA Contract number 13528/99/NL/MV, which was completed in 2001 and reported in ref. i.

1.1.2 This research divides into three major elements. Firstly a study of memory mapping and MBU hunting. Secondly, development of a technique for measuring the variation in SEE sensitivity with depth into the silicon of an IC by using laser testing at multiple wavelengths. Finally, an investigation of PWM SEE sensitivity, exploiting the special capability of lasers to pinpoint the location of SEE sensitive sites on the microchip dies. All these strands are connected by their utilization of MBDA's SEREEL laser SEE facility, which is described in the next sub-section.

1.2 The SEREEL Facility

1.2.1 The MBDA laser SEE testing facility (known as SEREEL) is shown in the configuration used for the present work in Figs. 1.1 and 1.2. The same facility has previously been used for the research reported in refs. i, vi and vii. The Neodymium-YAG picosecond pulse laser produces wavelengths of 1064nm or (with a frequency doubler) 532nm. Intermediate wavelengths are obtained by passing the green (532nm) pulses through a Raman tube of pressurised gas. Nitrogen was the gas species for this work. It generates wavelengths at 607nm and 707nm in its first and second order Stokes lines respectively. Each Stokes line may be selected onto an output mirror using a rotating Pellin-Broca prism. The 707nm wavelength in the visible red region of the spectrum was principally utilised for this work, since it penetrates the silicon to a depth of the order of 10μm. However, a range of wavelengths was used for the investigation of the SEU sensitivity profile with depth into SRAM's. A microscope is used to focus the laser pulses onto the surfaces of the delidded microchips as diffraction limited spots. The spot diameter approaches (from above) the limit imposed by diffraction of the pulse out of its own cross-section. For our microscope this limit is slightly larger than the wavelength of the light. The pulse width used throughout the present experiments was 40ps.

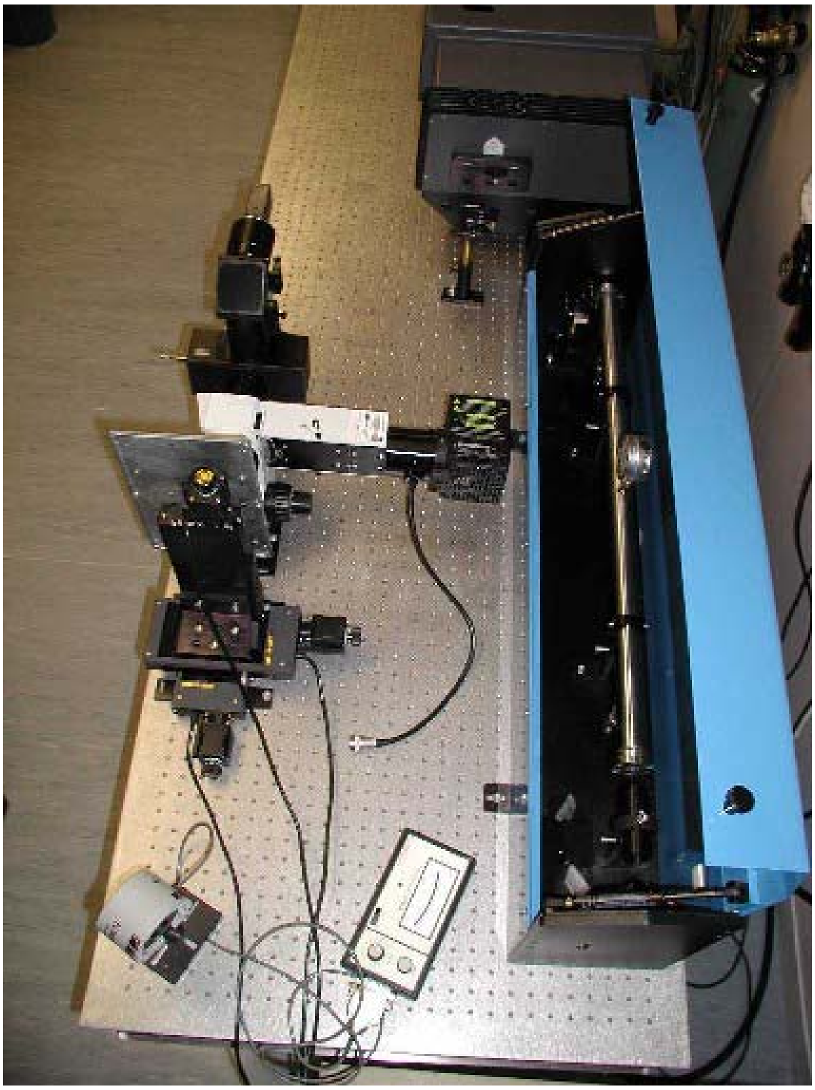

Figure 1.1. The Single Event Radiation Effects in Electronics Laser (SEREEL) Facility

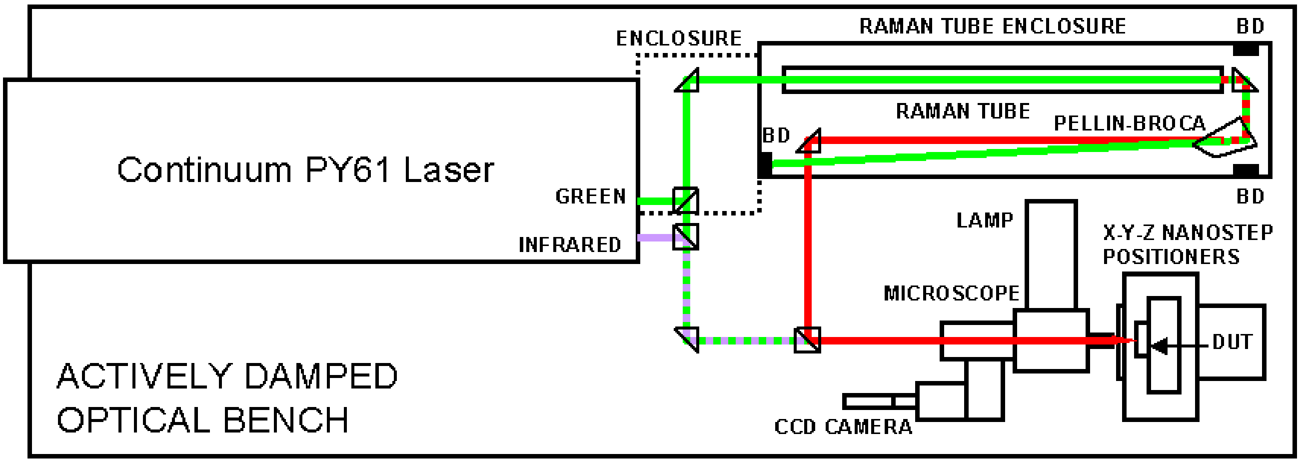

BD=BEAM DUMP, DUT=DEVICE UNDER TEST

Figure 1.2. Diagram of the laser SEE simulation facility (SEREEL).

2 REFERENCE DOCUMENTS

i) Utilisation Of Pulsed Laser For SEE Testing Study At Two Wavelengths, DR21738, ESA_QCA010801S_C, Andrew Chugg And Rodri Jones, MBDA, May 2001.

ii) Heavy Ion Single Event Effects In UCC1806 Pwm's, TOS-EPC/04.116/SI, Sven Landstroem And Reno Harboe Sørensen, ESTEC, 27th April 2004.

iii) Preliminary Heavy Ion Results Of UC1825A, UCL Heavy Ion Test Data From November 2004, P-JC10-MEM-00007-SE, Stanley Mattsson, Saab Ericsson Space, 1st December 2004

iv) P. C. Adell, R. D. Schrimpf, W. T. Holman, J. Boch, J. Stacey, P. Ribero, A. Sternberg And K. F. Galloway, "Total-Dose And Single-Event Effects In DC/DC Converter Control Circuitry," *IEEE Trans. Nucl. Sci.,* Vol. 50, No. 6, pp. 1867-1872, December 2003.

v) P. C. Adell, R. D. Schrimpf, B. K. Choi, W. T. Holman, J. P. Attwood, C. R. Cirba And K. F. Galloway, "Total-Dose And Single-Event Effects In Switching DC/DC Power Converters," *IEEE Trans. Nucl. Sci.,* Vol. 49, No. 6, pp. 3217-3221, December 2002.

vi) R. Jones, A. M. Chugg, C. M. S. Jones, P. H. Duncan, C. S. Dyer And C. Sanderson, "Comparison Between SRAM Cross-Sections From Ion Beam Testing With Those Obtained Using A New Picosecond Pulsed Laser Facility," *IEEE Trans. Nuc. Sci.*, Vol. 47, No. 3, June 2000.

vii) A. M. Chugg, R. Jones, M. J. Moutrie, C. S. Dyer, C. Sanderson And A. Wraight, "Probing The Charge Collection Sensitivity Profile Using A Picosecond Pulsed Laser At A Range Of Wavelengths," *IEEE Trans. Nucl. Sci.,* Vol. 49, No. 6, pp. 2969-2976, December 2002.

viii) C. Barillot, J. P. Bensoussan And P. Calvel, "Total Dose And Heavy Ions Evaluation Of UC1806 Pulse Width Modulator From Unitrode," *IEEE Radiation Effects Data Workshop*, pp. 55-59, 1995.

ix) A. M. Chugg, M. J. Moutrie And R. Jones, "Broadening Of The Variance Of The Number Of Upsets In A Read-Cycle By MBU's", *IEEE Trans. On Nucl. Sci*., Vol. 51, No. 6, December 2004.

3 MEMORY MAPPING AND MBU HUNTING

3.1 Introduction

3.1.1 Laser testing of the same set of commercial 1 Mbit SRAM memory devices as used in Phase 1 (ref. i) of this study was begun in February 2004. This work began with the calculation of memory maps for some of the devices and application of the memory maps to detect MBU's. This work and the new techniques developed within it are reported in this section.

3.2 Memory Maps

3.2.1 As an example of the application of a memory map derived under this study using SEREEL, the ion beam upsets recorded for the Cypress CY7C109 (0.65μm feature size version) under Phase 1 have been plotted using the new, laser-derived memory map. Errors in a sub-section of the memory are plotted for several different ion LET's and beam inclinations in Figures 3.1a to 3.1d. For this device, the bits of a data word are found to be widely spaced over the die surface, so MBU's within a single data word were not seen. However, the memory maps of the errors reveal that large MBU clusters were in fact occurring. Furthermore, although few MBU's were evident for 1MeV cm^2/mg ions, the proportion and size of MBU clusters increased markedly with ion LET. For 34MeV cm^2/mg ions (Figure 3.1d) there are some very extensive and pseudo-regular patches of MBU's (one, two and three adjacent short columns). These may be control logic errors or incipient latchups, since this device was observed to latchup at 14MeV cm^2/mg and above (though not in the read cycles from which the plotted data were obtained). There are indications that the MBU clusters grew horizontally when the ions were obliquely incident (e.g. Figure 1c), but the memory map may not be perfect at the finest spatial scale. Techniques for improving the fine scale correctness of the memory maps will be discussed in ensuing sub-sections.

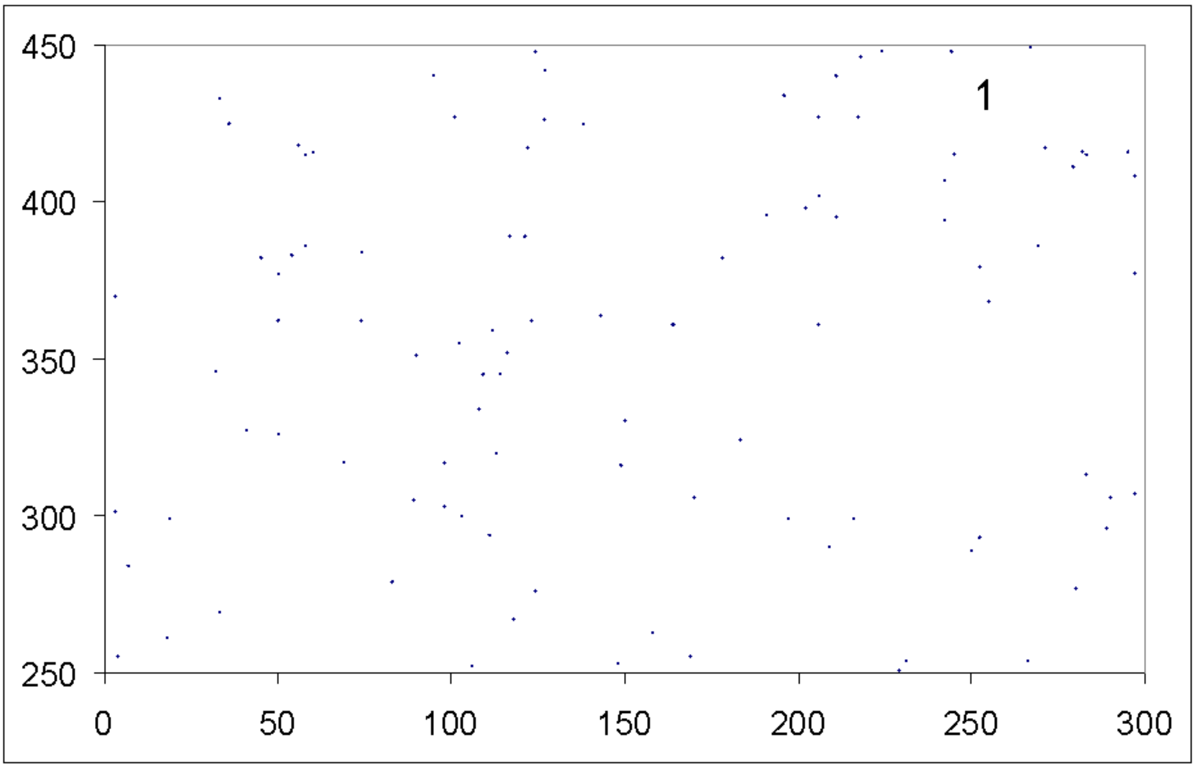

Figure 3.1a. Map of errors for 1 MeV cm^2/mg ions in the Cypress CY7C109 (0.65μm feature size) – ion data from Phase 1 plotted with a new (Phase 2) laser generated memory map.

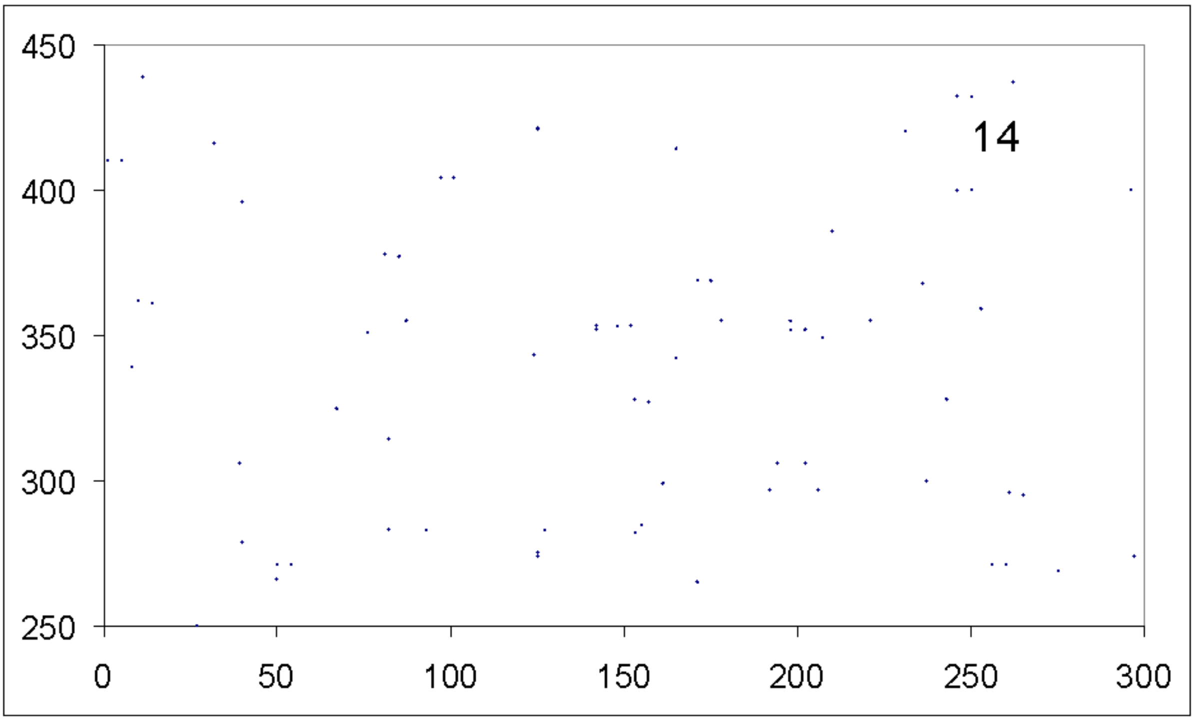

Figure 3.1b. Map of errors for 14 MeV cm^2/mg ions in the Cypress CY7C109 (0.65μm feature size) – ion data from Phase 1 plotted with a new (Phase 2) laser generated memory map.

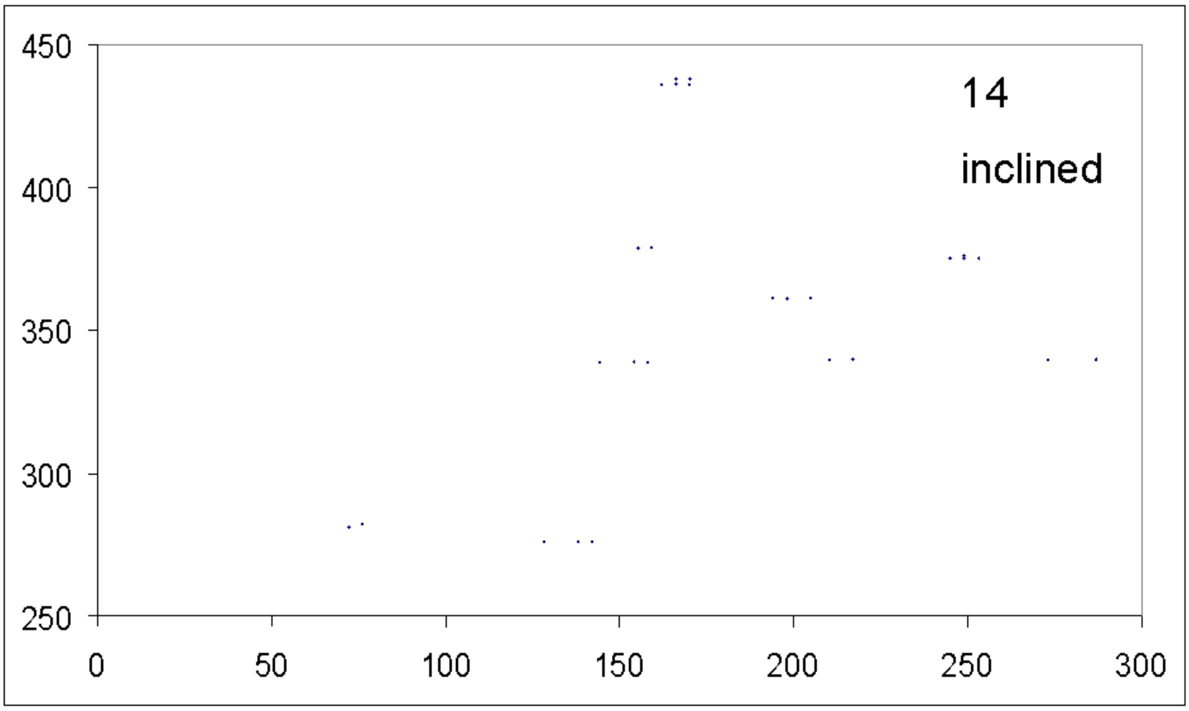

Figure 3.1c. Map of errors for 14 MeV cm^2/mg ions at oblique incidence in the Cypress CY7C109 (0.65μm feature size) – ion data from Phase 1 plotted with a new (Phase 2) laser generated memory map.

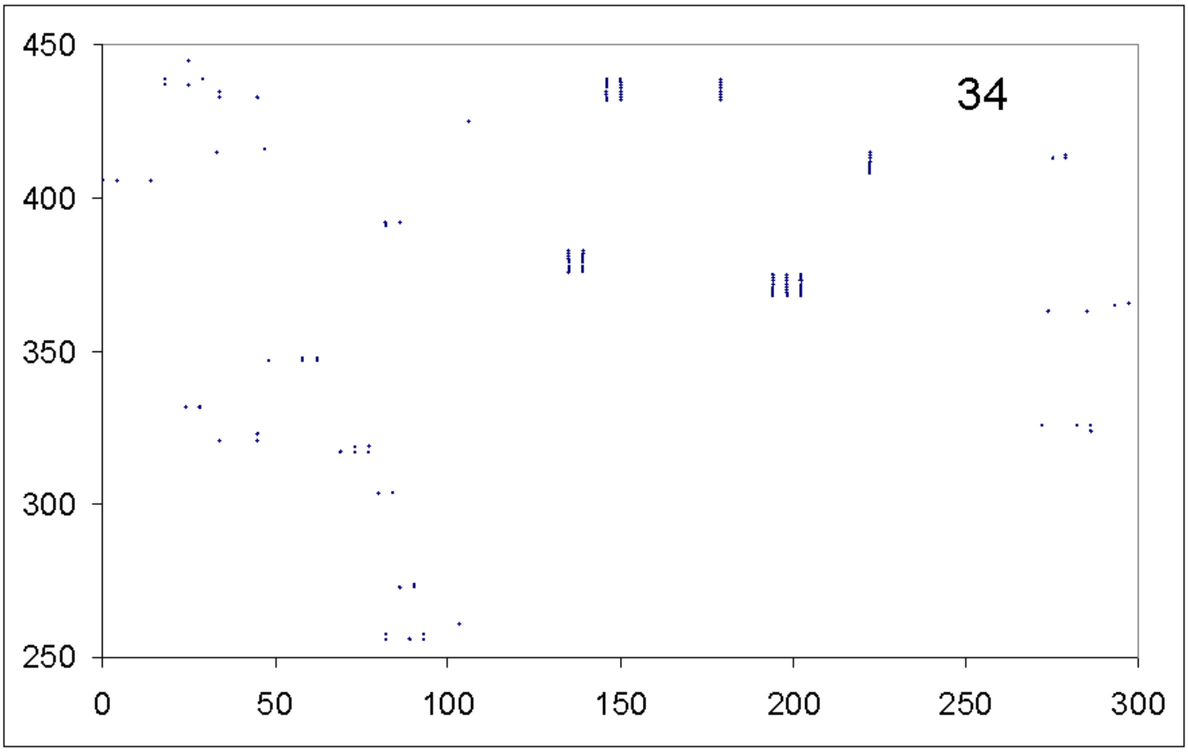

Figure 3.1d. Map of errors for 34 MeV cm^2/mg ions in the Cypress CY7C109 (0.65μm feature size) – ion data from Phase 1 plotted with a new (Phase 2) laser generated memory map.

3.3 Memory Mapping Techniques

3.3.1 In the previous sub-section the work was illustrated using Cypress CY7C109 laser measurements. In this section we will use results from laser testing of the Mitsubishi M5M51008B. In this work we have evolved more efficient approaches to laser memory mapping, because it has been found that memory mapping using a straightforward pulse-by-pulse approach can be unreasonably time-consuming. The most efficient approach developed is to deliver an array of small patches of laser errors to the device. The array needs to be irregular with a higher density of patches in some areas: it is best understood through the example of its application to the Mitsubishi M5M51008B.

3.3.2 For each error patch we obtain a list of a few tens of addresses containing (usually) one upset bit. It is possible to add together the values of each bit of the address to form charts for each error patch, examples of which are given in Figures 3.2 and 3.3. These address bit sums are given in columns 0 to 16. It is also possible to identify which bit has been upset at each upset address and this bit can be designated with a three bit "nibble" (part of a byte) in the range 0 to 7. These three bits can also be treated as an extension of the byte address to form the specific bit address and they have also been summed in columns 25 to 27 of Figures 3.2 and 3.3 (although these columns are all zero in Figure 3.3, this is still significant, because it means that all the upset bits in this error patch [P] were bit 0 of the data word; conversely, almost all the upsets were for bit 2 in Figure 3.2).

3.3.3 It will be apparent that within each error patch the error bit sum is approximately zero or approximately equal to the number of errors in the patch for most bits of the address. However, for 5 or 6 of the address bits, these sums have intermediate values. These 5 or 6 bits are those that control very fine scale positioning in the memory map, but the other bits which are consistently one or zero within the patch are responsible for large scale positioning within the map. For these latter address bits, we have plotted charts locating the 18 error patches on the die surface: blue diamonds indicate that the bit was generally 0 for that patch and red squares indicate 1's. As an example, the patch map for bit 1 of the address is shown in Figure 3.4. It is immediately obvious from the overall pattern that bit 1 is always constant in the horizontal sense, but flips every one eighth of the die in the vertical sense. This tells us the positioning information, which derives from this bit. The overall memory map is the assemblage of such bit information for all the address and data-address bits. Thus we have plotted graphs like Figure 3.4 for all the bits, which were found to have consistent values within each error patch. This resolves the memory map down to the last 5 or 6 bits.

3.3.4 The last few bits are not very important for finding MBU's, because they control spacing differences which are small compared with the random spacing of upsets across the die. In other words, the higher order bits are sufficient to get the bits of MBU's close enough together that they can be recognised. We have therefore been developing a quick, but not always 100% accurate method of ordering the lowest 6 bits of the address (bits 0, 2,3,4,5, 6 for the Mitsubishi M5M51008B).

3.3.5 The low bit sorting technique is based on the fact that it is computationally feasible to try all possible permutations for the lowest 6 to 8 bits of the address within a few minutes on a PC. All that is necessary is to define a criterion by which the best permutation can be identified. In fact we have adopted two different criteria, depending on the nature of the distribution of error bits that we are feeding into the search algorithm.

3.3.6 If we have an even distribution of errors from ion/proton/neutron testing which also contains some MBU's, then the correct permutation of the lowest order bits will be that which brings the members of the MBU's together as closely as possible in the map (Figure 3.5). This permutation will also give a minimum sum for the nearest neighbour distances between errors, because the MBU's will give especially low nearest neighbour distances.

3.3.7 However, if we have a round patch of errors from a single defocused laser pulse, the nearest neighbour distances method does not work, because it does not favour a circular patch (correct) over an elliptical or lenticular patch or some other splodge, where the error bits are all adjacent (incorrect). In this case the circular patch will minimise the sum of the distances between each bit and each other bit in the error patch (Figure 3.6).

3.3.8 At this point, we have achieved an ordering of the address bits and a decision as to whether they control x or y positioning. This gives two groups of address bits that can be used to generate x and y co-ordinates for the location of each error in the memory map. We can now test this basic memory map by plotting each of the errors in the laser error patches to their corresponding (x,y) co-ordinates in a graph over the microchip die (Figure 3.7). In this case for multiple error patches minimising the sum of nearest neighbour distances was found to work best.

3.3.9 It can be seen that some of the error patches are split into two groups. It can also be seen that the splits generally occur at significant powers or multiples of two in the y-direction, e.g. y = 512 = 2^9. This phenomenon is due to the common practice of mirroring or rotating (or both) every other memory block. Manufacturers seem frequently to do this for memory blocks on a variety of scales. It can be very complicated to work out all these modulations of the basic bit ordering in the memory map. It is also generally not very important for the location of MBU's, because it will be relatively rare for MBU's to be split over memory block boundaries. (Note that there are also a few stray errors not apparently related to the error patches – these may reflect some type of occasional control logic upset.)

3.3.10 At this point we can try plotting our ion beam test data for the Mitsubishi M5M51008B according to the calculated memory map. A sub-section of the resulting error map for 34 MeV cm^2/mg ions is shown in Figure 3.8. A very large proportion of many-bit MBU's is manifested (as was also shown for the Cypress CY7C109 device in the previous sub-section). This tends to confirm the efficacy of these laser memory mapping techniques.

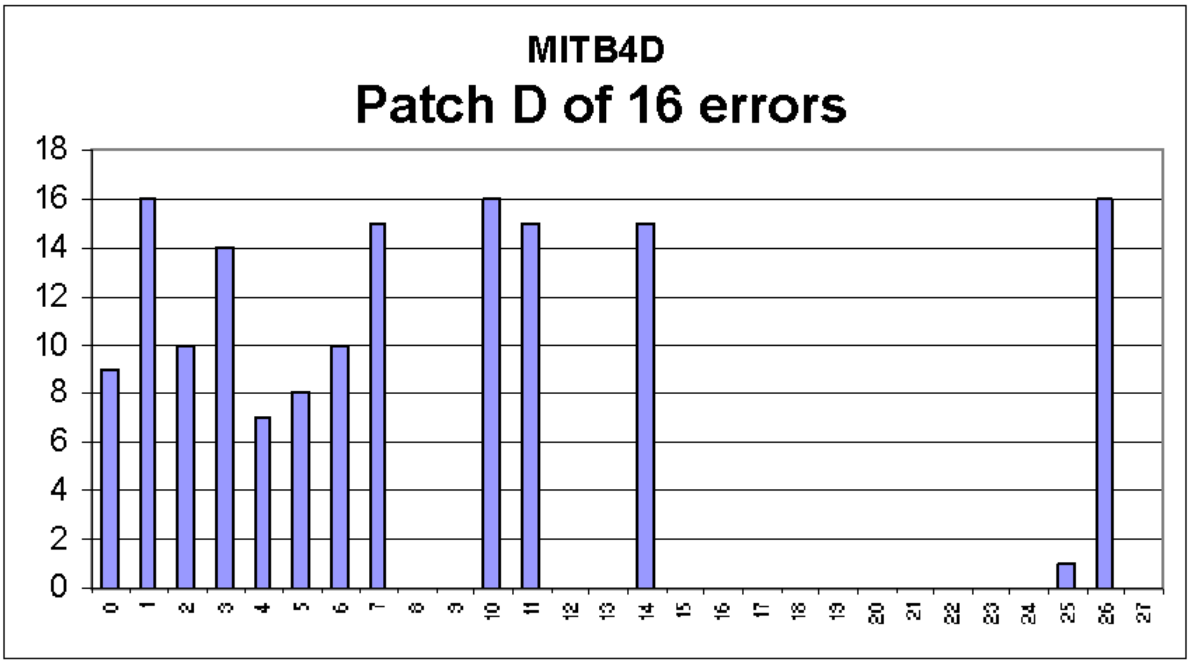

Figure 3.2. Address bit sums for laser patch D

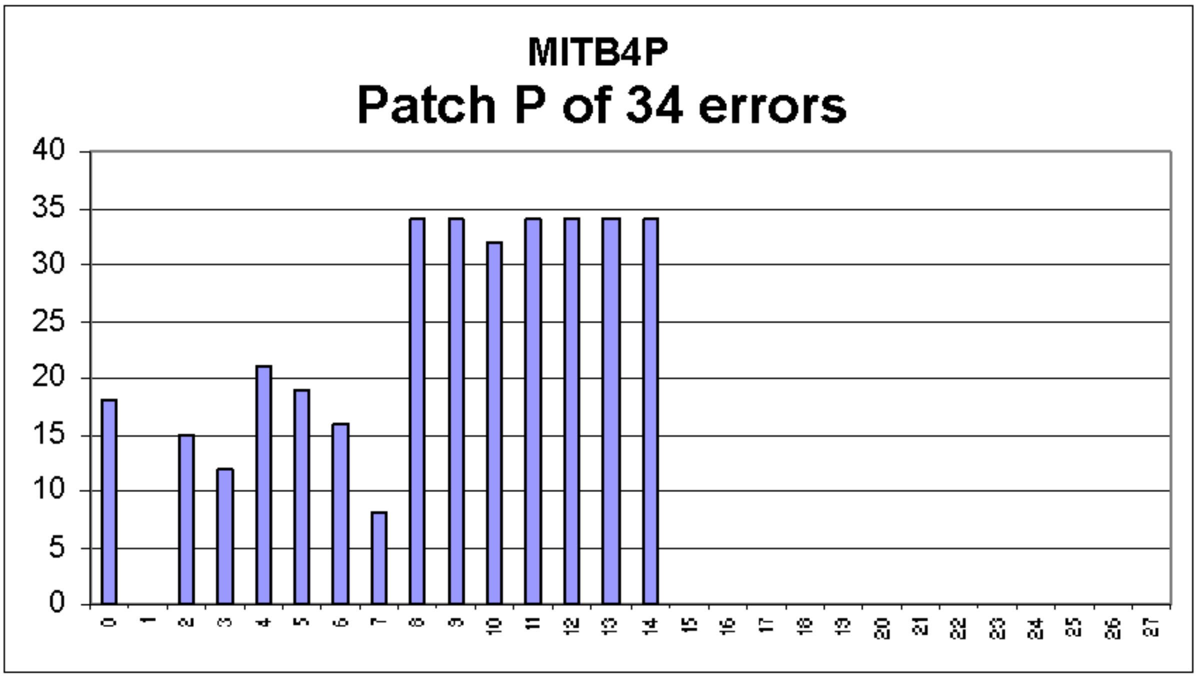

Figure 3.3. Address bit sums for laser patch P

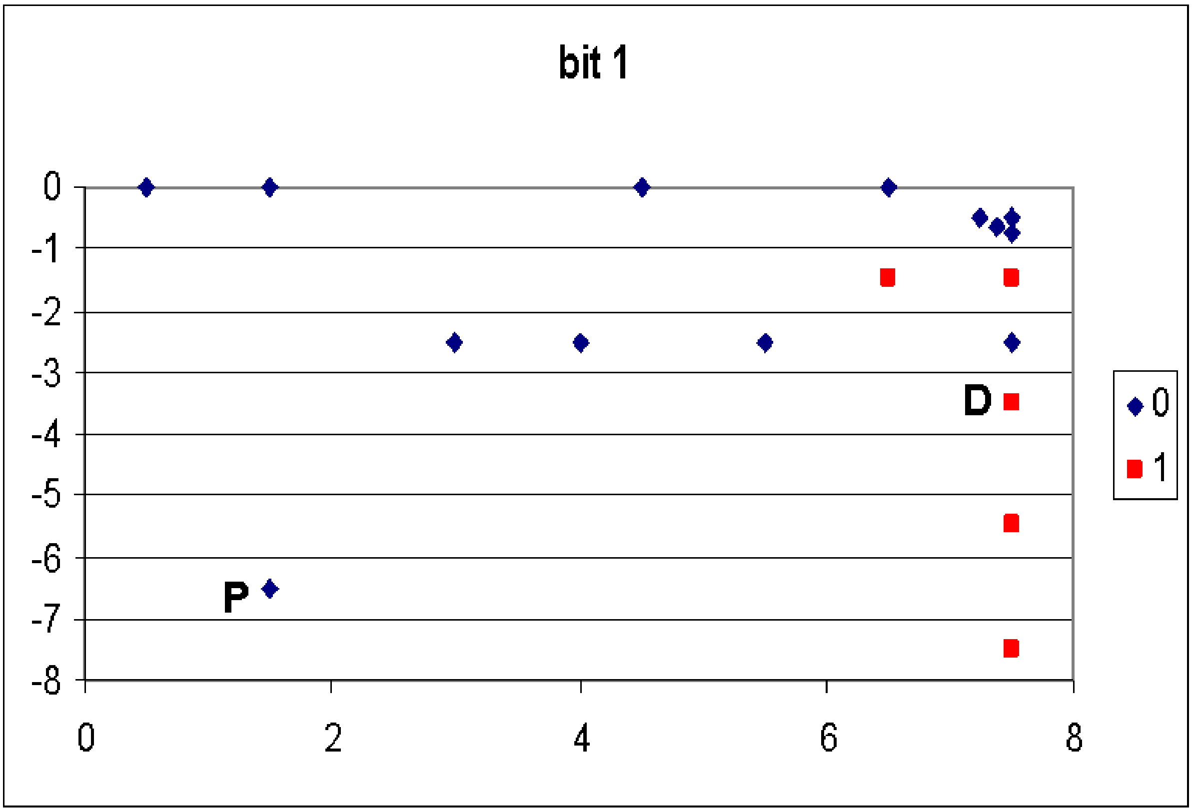

Figure 3.4. Bit 1 laser patch error map

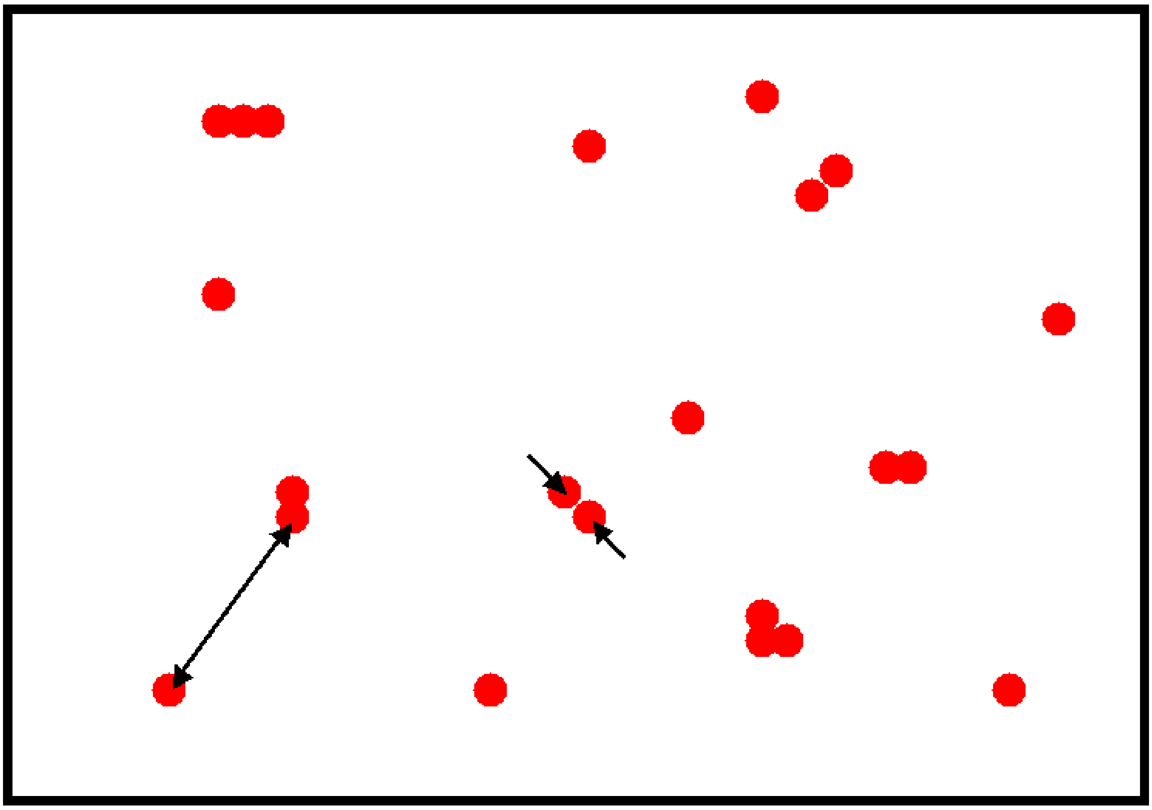

Figure 3.5. Minimising the sum of distances to nearest neighbours method of ordering lowest bits

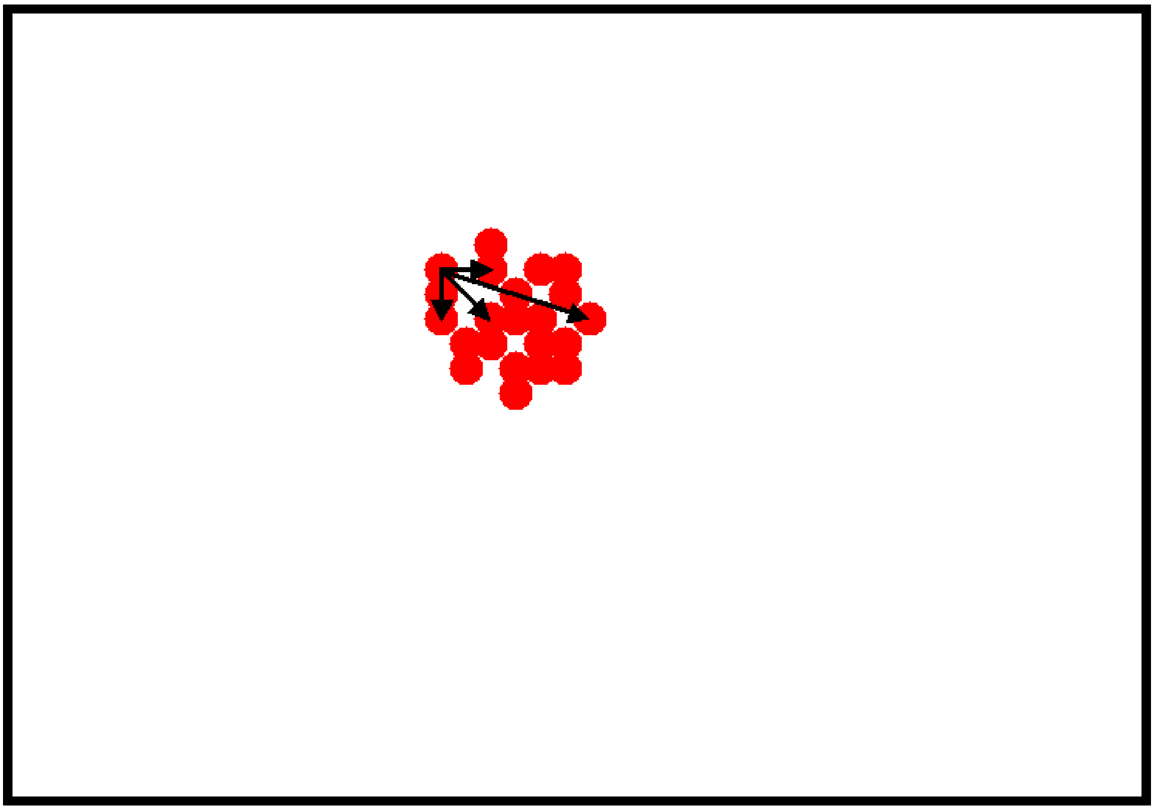

Figure 3.6. Minimising the sum of distances to all neighbours method of ordering lowest bits

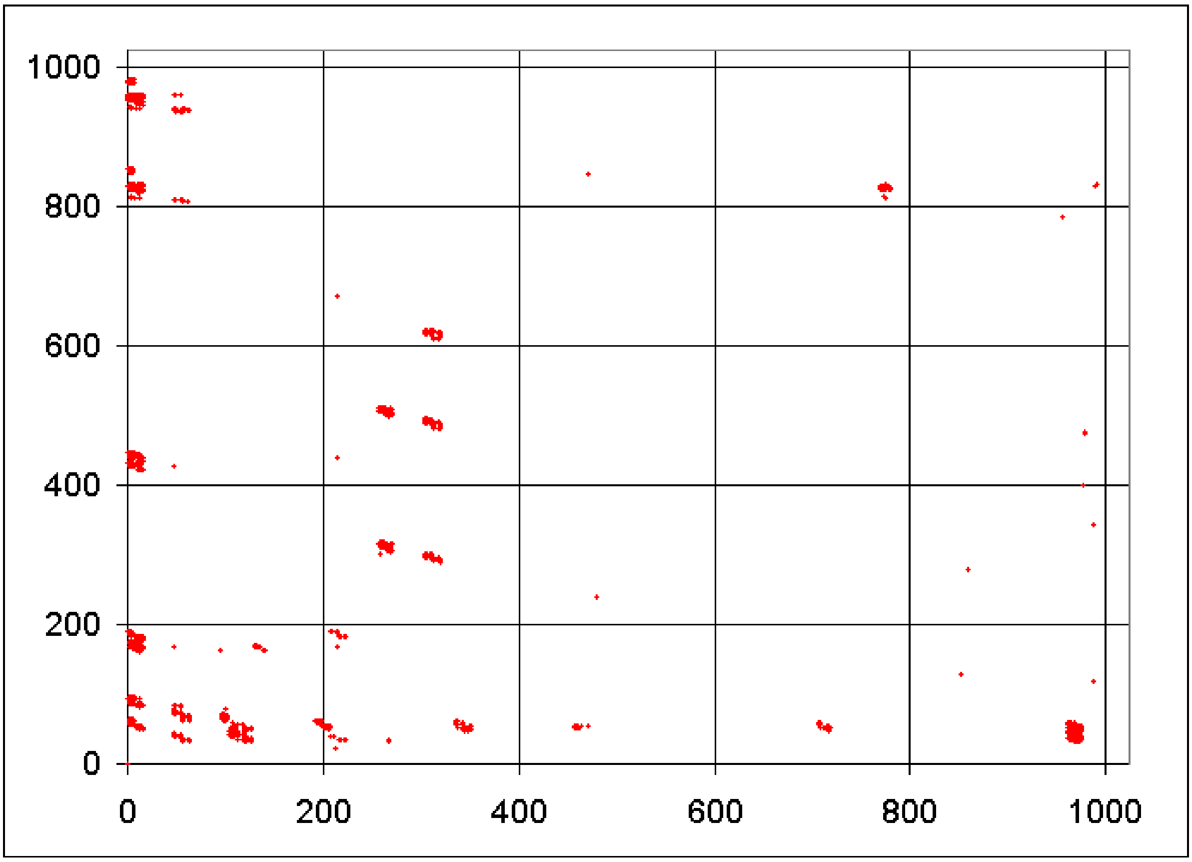

Figure 3.7. Plotting the laser error patches using the derived memory map

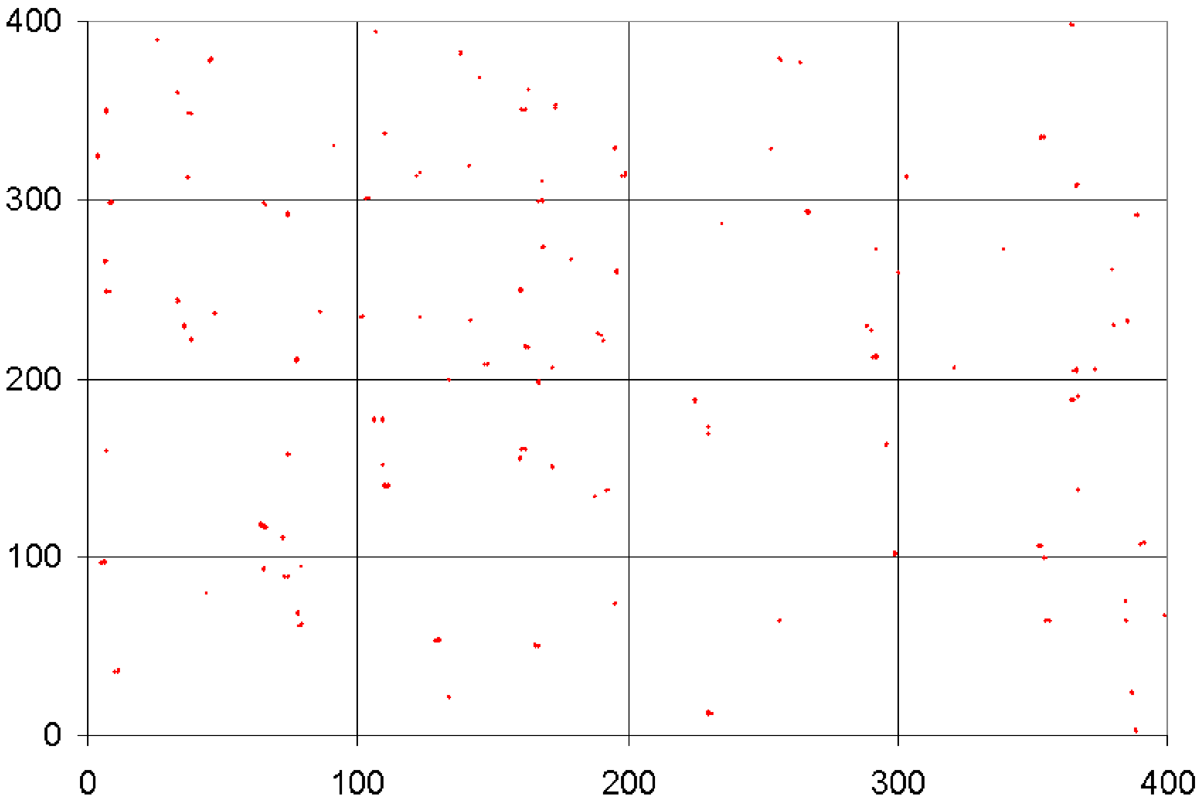

Figure 3.8. Plotting ion induced errors in the Mitsubishi M5M51008B at 34 MeV cm^2/mg using the derived memory map

3.4 MBU Analysis Techniques

3.4.1 In our NSREC 2004 paper, "Broadening of the Variance of the Number of Upsets in a Read-Cycle by MBU's" (ref. ix), we presented a new technique for determining the proportion of MBU's in SEE test data by analysing the statistics (variance and mean) of the numbers of errors in each memory read-cycle. It is apposite to investigate the application of this new technique to the ESA Laser SEE study data. We have therefore re-analysed the Cypress CY7C109 data using this technique, since we have previously found from laser SEE mapping that the number of MBU's increases steeply with LET for this device. In Figure 3.9 we have plotted the ratio of the variance:mean of the number of upsets as a function of LET. The increase in the variance predicted by the new technique is clear to see in these data.

3.4.2 However, we know from our laser MBU analysis that there were almost no MBU's at 1 MeV cm^2/mg, so the variance should have been equal to the mean at this point. In fact it was nearly twice as large, which implies that the ion beam flux was varying from one read-cycle to the next. This ion beam instability needs to be factored out of the data in order to discern the part of the variance broadening caused by MBU's. Fortunately, we can use the 1 MeV cm^2/mg data to get a measure of the degree of ion beam flux instability, because that is the only significant source of variance broadening at that LET.

3.4.3 Firstly, we need to define the maths for factoring out the flux variations. If the mean number of upsets per read-cycle is μ_M, the upsets per unit fluence is μ_F and the fluence per read-cycle is μ_Ψ, then:

$$\mu_M = \mu_F \mu_\psi$$

It is a text-book result that the standard errors for the values in this product are related to one another by:

$$\left[\frac{\sigma_M}{\mu_M}\right]^2 = \left[\frac{\sigma_F}{\mu_F}\right]^2 + \left[\frac{\sigma_\Psi}{\mu_\psi}\right]^2$$

To simplify the calculations we can define the mean fluence delivered during a read-cycle to be one "unit". Using the 1 MeV cm^2/mg data, σ_F^2 is approximately equal to μ_F, because there are very few MBU's, and μ_F may be approximated by μ_M, hence we obtain an estimate of σ_Ψ:

$$\sigma_\Psi = \sqrt{\left[\frac{\sigma_M}{\mu_M}\right]^2 - \frac{1}{\mu_M}}$$

This gives a standard deviation for the ion beam flux of about 4.1%. The actual variations in the number of upsets recorded in each read-cycle at this LET are shown in Figure 3.10. We can now proceed to derive values of σ_F and μ_F using data values at an LET of 5 MeV cm^2/mg (at which we know there are numerous MBU's). We can try our formula derived in the NSREC paper to calculate the mean upsets per event μ_N:

$$\mu_N = \frac{2 - 3\mu_F + \sqrt{(3\mu_F - 2)^2 + 8(\sigma_F^2 + 2\mu_F)}}{4}$$

This gives 1.85 upsets per event. However, the calculation is subject to an error margin of the reciprocal of the square root of the number of read-cycles. Since we only have 16 read-cycles for this data (Figure 3.11), the error margin is 25%, so our result is correctly stated as 1.85 $\pm$ 0.46. We can use our laser-derived memory map (Figure 3.12) to check the actual number of upsets per event and this value is approximately 1.36. The two values are therefore within the intrinsic error margins of the calculations, but this is not a very good test, because too few read-cycles of data are available for the calculations to be accurate. It should also be mentioned that the last equation cited assumes the MBU distribution is similar to that seen in neutron beam testing. The form could be different for ions, which would give an additional systematic error.

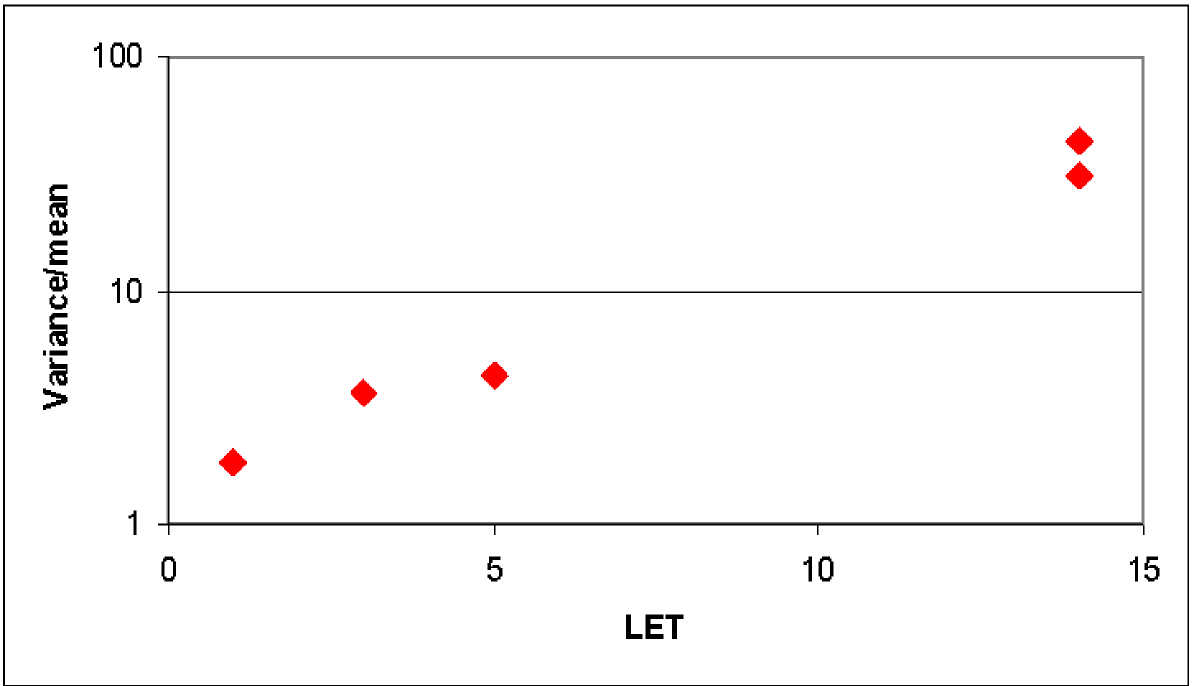

Figure 3.9. Broadening of the variance of the upsets per read-cycle with increasing LET

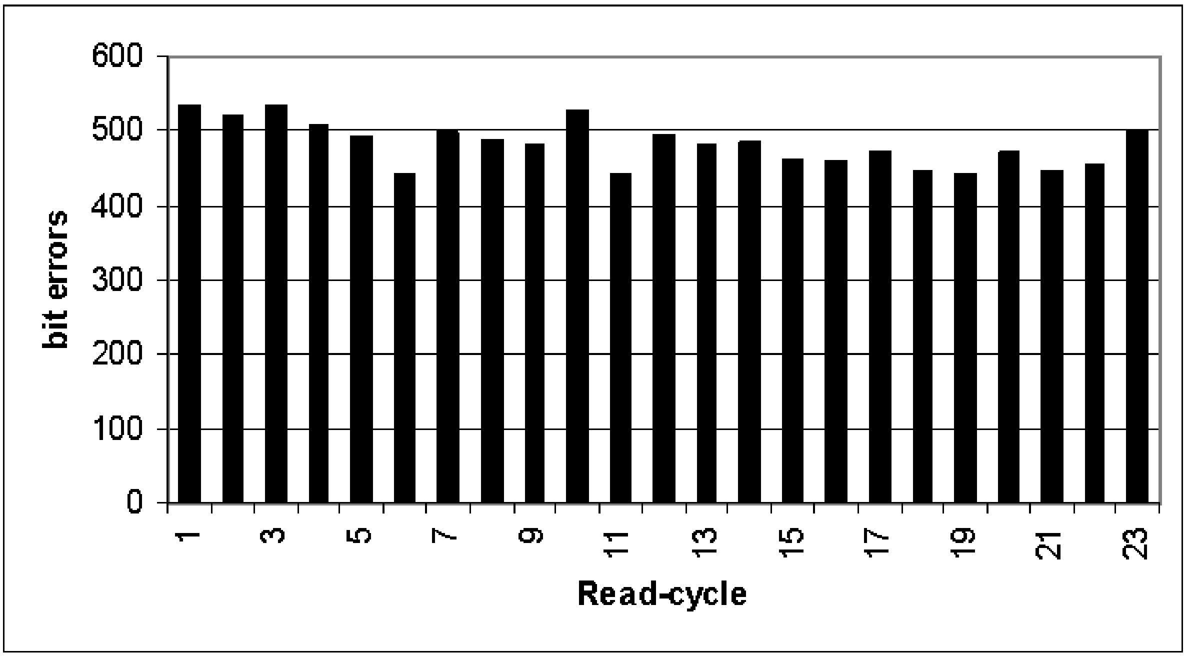

Figure 3.10. Actual numbers of errors in each read-cycle for the CY7C109 at 1 MeV cm^2/mg

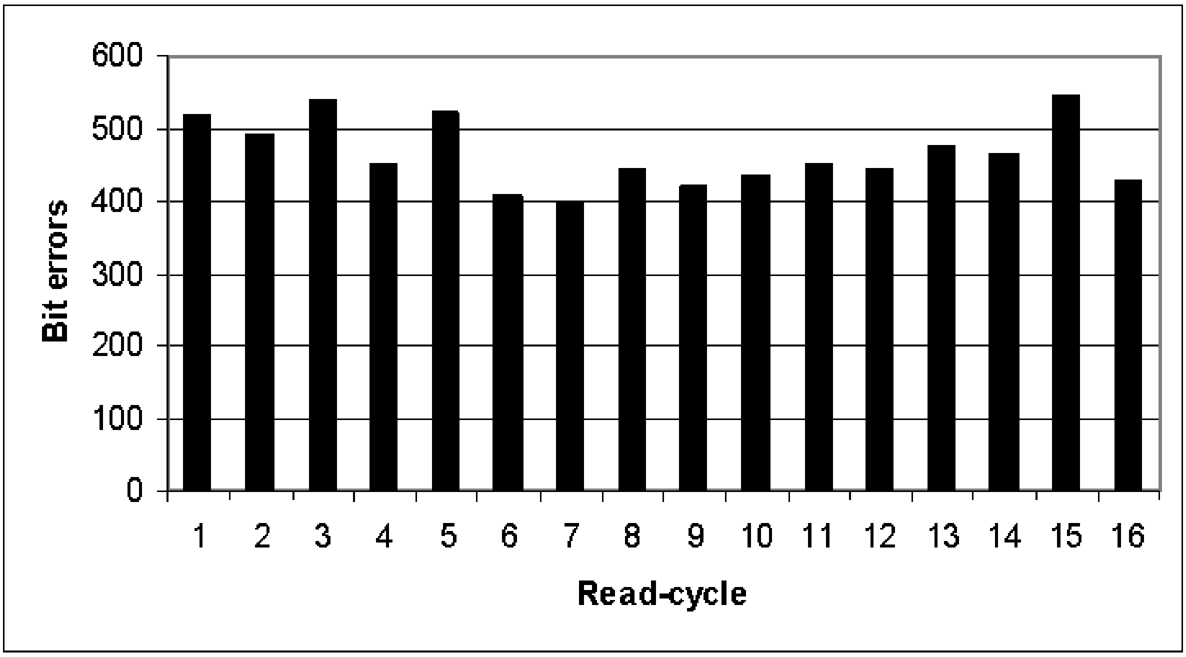

Figure 3.11. Actual numbers of errors in each read-cycle for the CY7C109 at 5 MeV cm^2/mg

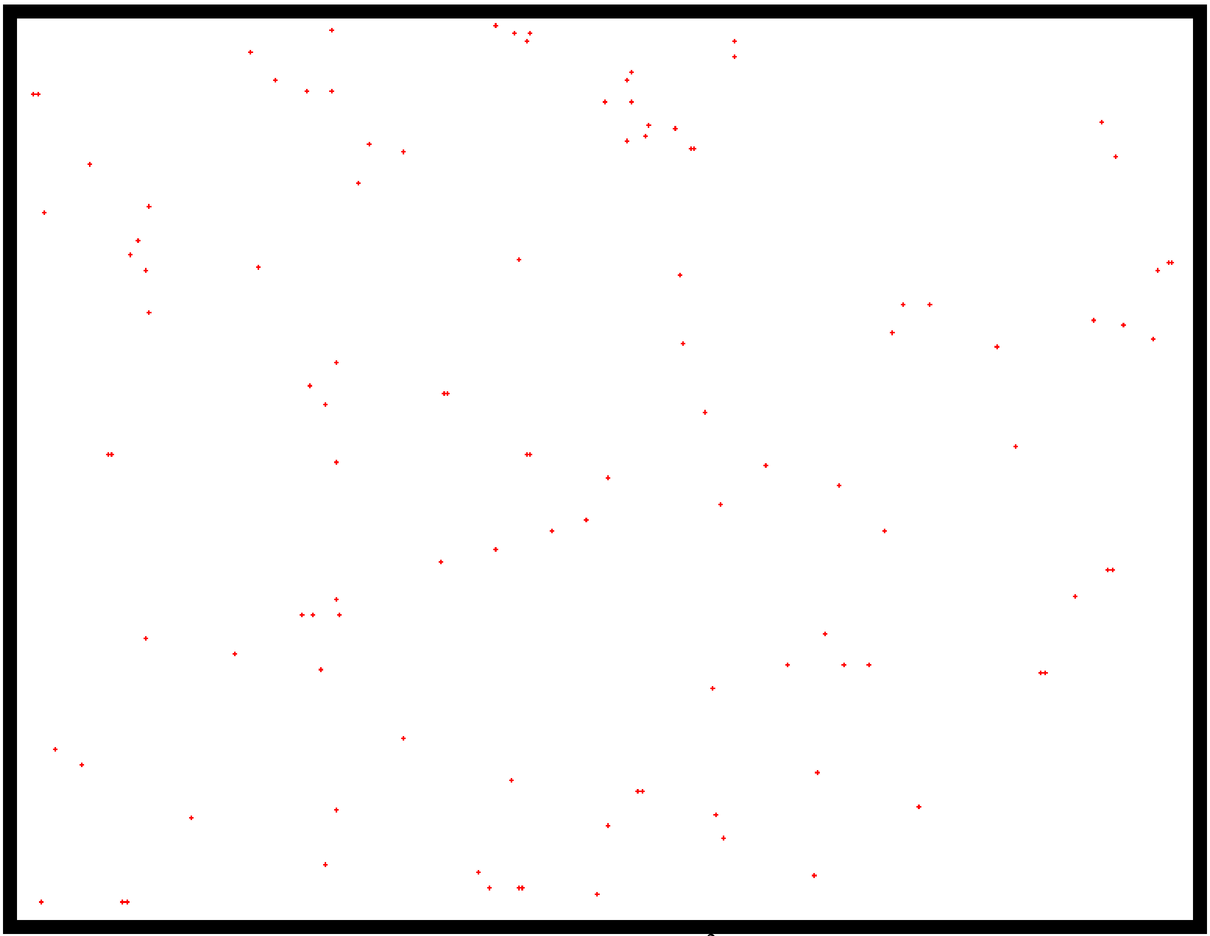

Figure 3.12. Upsets in the CY7C109 at 5 MeV cm^2/mg using the laser-derived memory map.

4 MULTI-WAVELENGTH LASER SEE TESTING

4.1 Introduction

4.1.1 This section will concentrate on the measurement of the variation in SEE sensitivity with depth into devices by applying a multi-wavelength technique to the samples of the 1Mbit memory devices utilised in Phase 1 of this study (ref. i). This has been performed using the SEREEL laser system to measure the SEE cross-section at four different wavelengths. The variation in the threshold laser pulse energy with wavelength provides information on the variation in SEE sensitivity with depth, because the penetration of laser light into the silicon increases with increasing wavelength.

4.2 Measuring SEE Sensitivity Variations with Depth

4.2.1 The SEREEL facility has been used to measure the SEE upset thresholds of the Cypress CY7C109 (0.42μm feature size) and Mitsubishi M5M51008B SRAM's at four laser wavelengths: 532nm (green), 607nm (green-yellow), 707nm (red) and 1064nm (infrared). The pulse energies have been measured directly using a new technique where the laser is defocused onto a sensitive CCD device for a few seconds. The resultant image of a laser light patch (Figure 4.1) can be integrated to measure the total light energy deposited in the CCD. The integrated signal from a control frame (laser light blocked) is then subtracted to remove the dark current signal and any stray light (though the testing was conducted in a dark room). This technique gives much better absolute measurements of laser pulse energy than the previous method, which relied on measuring the intensity of the main laser beam with a calorimeter, then scaling the energy down by around 6 to 8 orders of magnitude using multiple neutral density filters. The relative accuracy of pulse measurement is also improved by the new technique, leaving a standard error of about 15% in the values (based on performing several measurements and calculating the standard deviation). Most of this error seems to be attributable to laser instability and should be removed when the new SEREEL2 laser is installed in the Spring of 2005.

4.2.2 The results are shown in Figures 4.2 and 4.3 respectively. It is desirable to define the threshold at some fixed number of errors in the middle of the range, because small numbers of errors are subject to large random statistical fluctuations and the cross-sections tend to flatten (saturate) at large numbers of errors. However, large numbers of errors were not seen for the Cypress device, because it repeatedly latched at about the 100 errors pulse energy level and above. Hence the Cypress threshold was defined at 30 errors in 1000 pulses. Conversely, the Mitsubishi chip exhibited exceptional sensitivity to infrared pulses at low error fractions, so its threshold was defined at 500 errors per 1000 pulses to offset this distorting effect. The thresholds for each device are given in Tables 4.1 and 4.2 respectively, together with the associated laser wavelengths and silicon absorptivities.

Wavelength (nm)	Threshold Energy (pJ)	Absorptivity (cm^{-1})	Laplace transform ($1/\alpha\lambda E_t$)
532	260	12500	5.78369E-10
607	340	6000	8.07572E-10
707	1150	2300	5.34755E-10
1064	8200	20	5.73079E-09

Table 4.1. Thresholds at four wavelengths for 30 errors in 1000 pulses for the Cypress CY7C109 (0.42μm version)

Wavelength (nm)	Threshold Energy (pJ)	Absorptivity (cm^{-1})	Laplace transform ($1/\alpha\lambda E_t$)
532	98	12500	1.53445E-09
607	100	6000	2.74574E-09
707	155	2300	3.96754E-09
1064	1700	20	2.76426E-08

Table 4.2. Thresholds at four wavelengths for 500 errors in 1000 pulses for the Mitsubishi M5M51008B

4.2.3 We have shown in our conference paper (ref. vii) that the thresholds E_t are related to the variation in charge collection efficiency CCE(x) with depth x into the silicon by a Laplace Transform:

$$\frac{hcQ_{crit}}{\lambda E_t \alpha} = \int_0^\infty CCE(x)\exp[-\alpha x]dx$$

Where α is the absorptivity at wavelength λ and Q_{crit} is the critical charge for upset to occur (assumed to be invariant with wavelength). It is only necessary to perform an inverse Laplace Transform on the four pairs of experimental data (E_t,λ) in order to derive a plot of CCE(x). A procedure for doing this has been described in our paper and has been applied to the results for the Cypress and Mitsubishi devices. The CCE profiles calculated by the inverse Laplace Transform method are shown in Figures 4.4 and 4.5.

4.2.4 The calculated CCE profiles exhibit some interesting features, which have important implications for SEE testing in general. Firstly, the results compel the interpretation that the CCE profiles have both positive and negative ranges. Given the demonstrable level of accuracy of the measurements, it is impossible to avoid the conclusion that the CCE profile must change sign with depth. This means literally that laser ionisation causes net electrons to flow onto the memory cell node when it is delivered at some depths, but electrons flow off the node when the ionisation happens at other depths.

4.2.5 An ion will generally plough through tens of microns of the silicon, so its net effect will depend on an average over both negative and positive ranges of the CCE profile. The thresholds for ion SEE should therefore be related to the integration of the profile over a large range of depth. Conversely, neutrons and protons will produce recoiling silicon nuclei, which typically have ranges of a micron or less. Consequently, the net effect of neutrons and protons will depend crucially on where they interacted within the CCE profile. In general, the threshold for proton and neutron SEE will depend on the peak value in the CCE profile. Since the integration of a profile which has positive and negative ranges will usually be uncorrelated with the peak value within the profile, the new laser results imply that proton and neutron SEE susceptibility will correlate rather poorly with ion SEE susceptibility. In general, there is plenty of evidence to suggest that this is indeed true in practice.

4.2.6 A second interesting feature is most pronounced in the results for the Mitsubishi device (Figure 4.5), which exhibits particularly high levels of CCE deep into the silicon. This feature of the CCE profile comes entirely from the abnormally low threshold for upset in this device at the infrared wavelength (Figure 4.3). Normally, the infrared threshold should be much higher than the visible light thresholds, because infrared pulses deliver a much lower LET for the same pulse energy. Furthermore, the slope of the infrared cross-section for the Mitsubishi device is much flatter than for visible wavelengths. The implication of this is that the infrared pulses are causing SEU by a different mechanism than the visible pulses and that this mechanism is causing charge to be drawn onto the node in large amounts from deep within the substrate of the microchip. There is only one obvious candidate for the cause of this phenomenon: the funnelling effect. (The reason funnelling is not caused by visible light pulses is that they do not penetrate deeply enough into the silicon.)

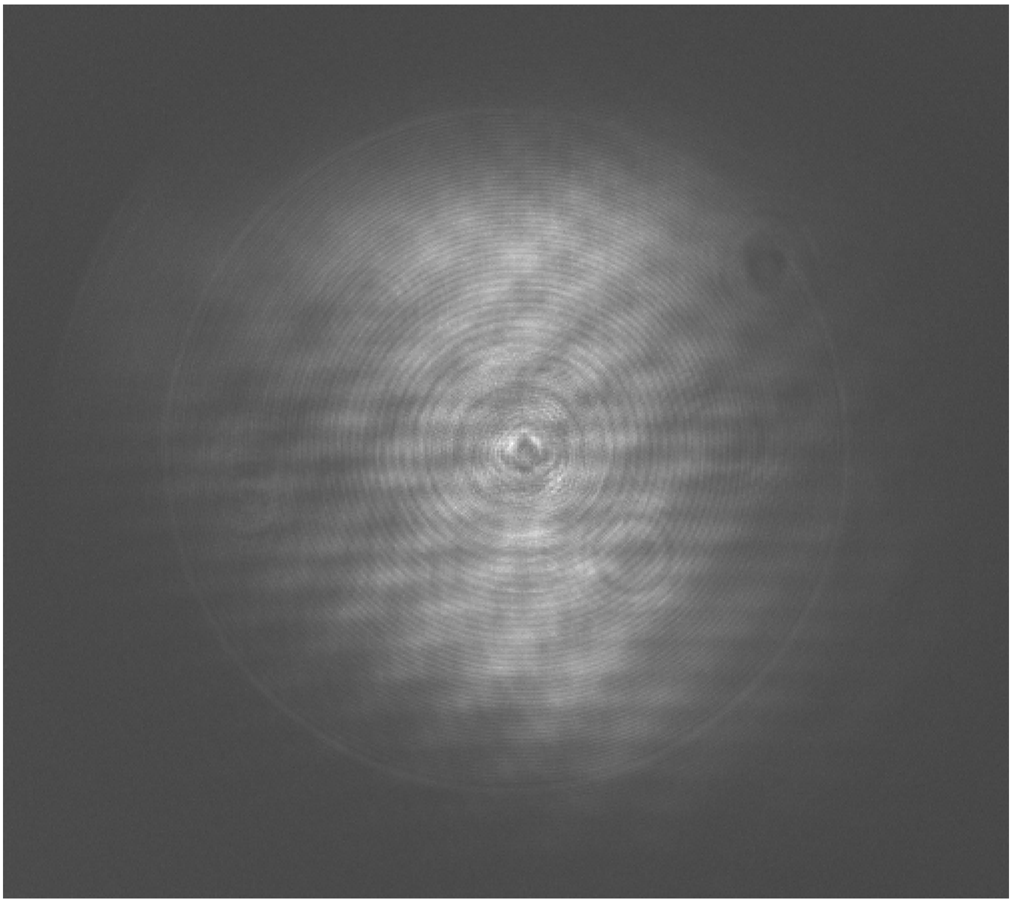

Figure 4.1. Defocused infrared laser pulses in the CCD camera - the rings and stripes are diffraction phenomena, which do not alter the net signal in the image

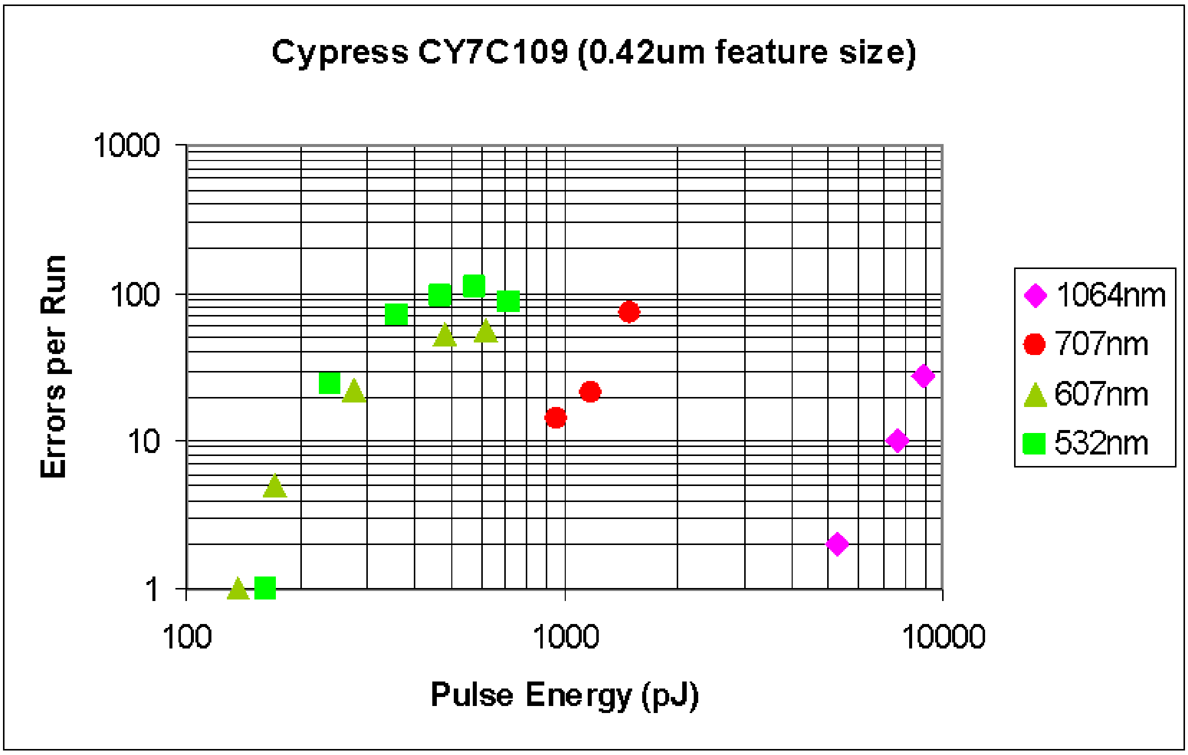

Figure 4.2. Laser SEE upset thresholds at four wavelengths for the Cypress CY7C109 (0.42μm version)

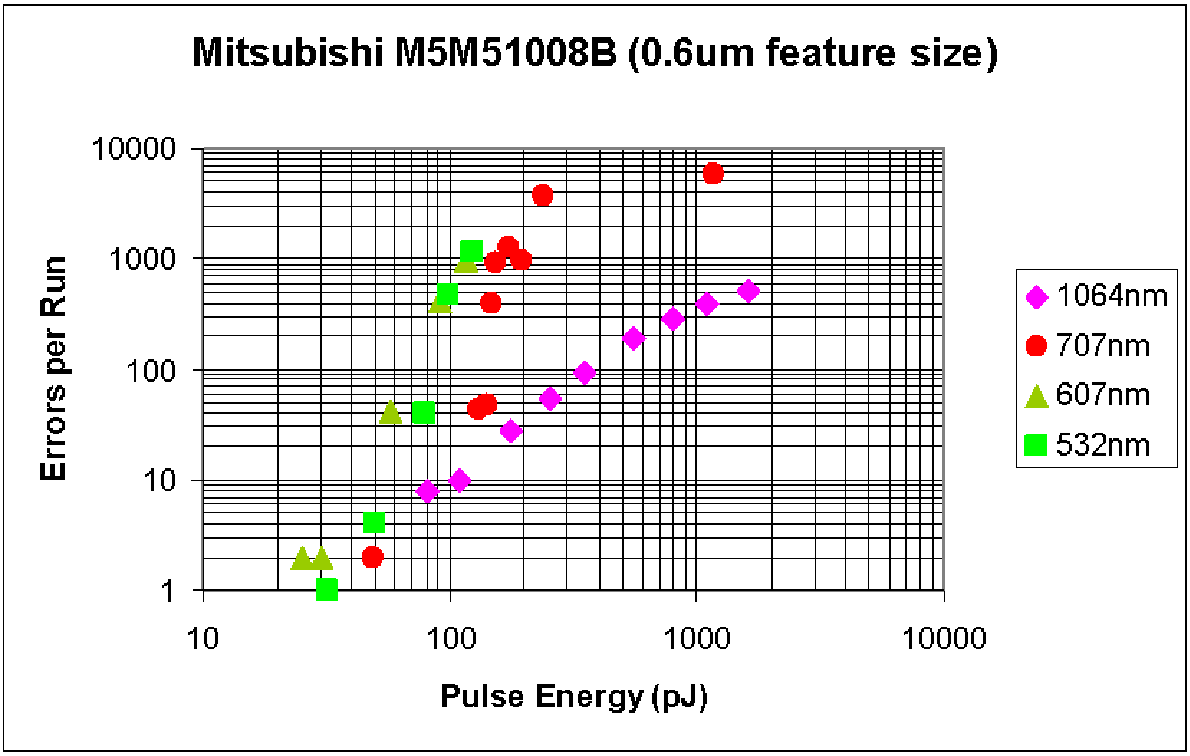

Figure 4.3. Laser SEE upset thresholds at four wavelengths for the Mitsubishi M5M51008B

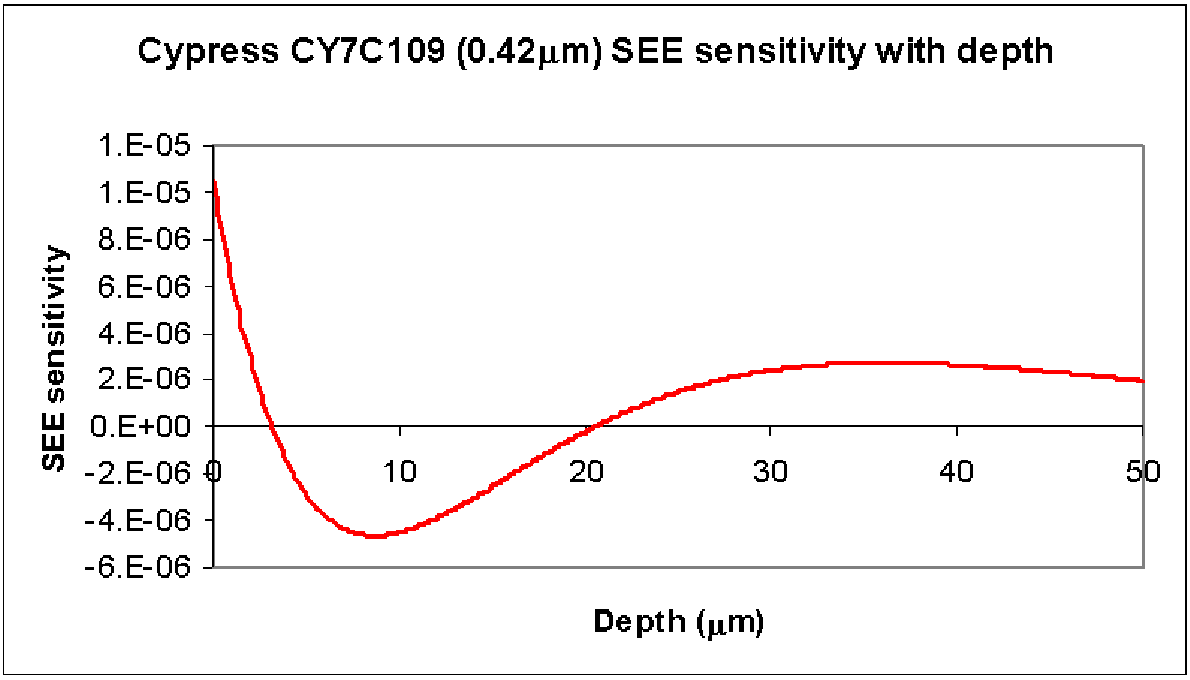

Figure 4.4. Calculated charge collection efficiency (SEE sensitivity) with depth into the silicon for the Cypress CY7C109 (0.42µm version)

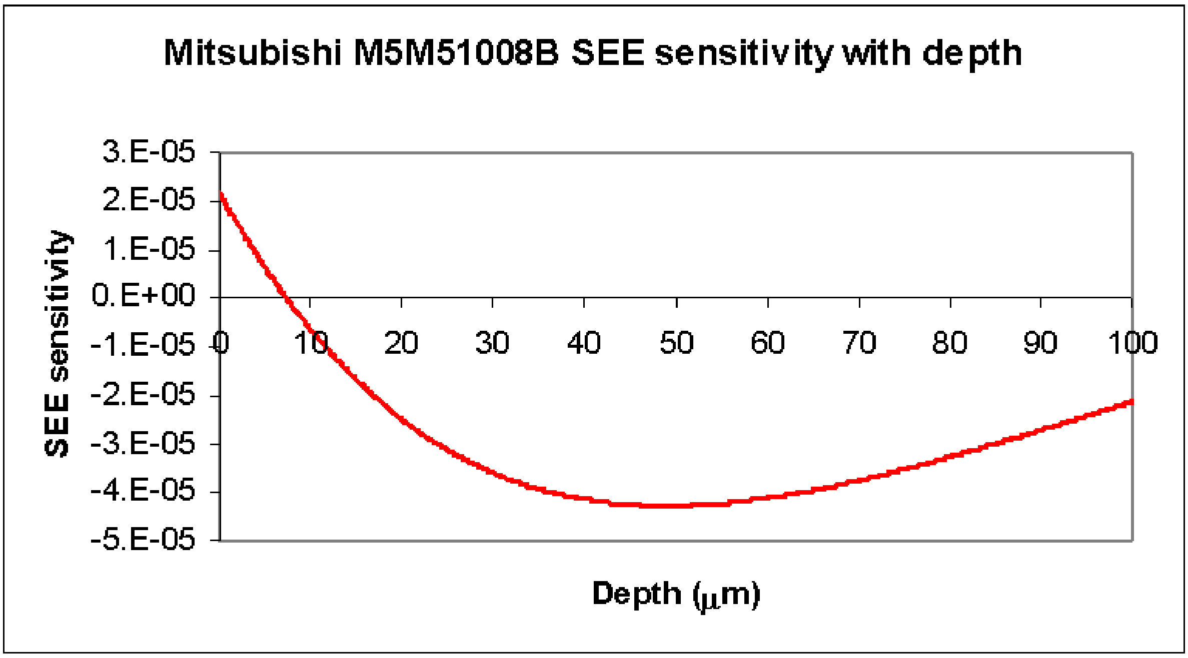

Figure 4.5. Calculated charge collection efficiency (SEE sensitivity) with depth into the silicon for the Mitsubishi M5M51008B

5 SEE PROBING OF PWM'S

5.1 Introduction

5.1.1 Recent operational experience (ref. ii) has shown that Pulse Width Modulators (PWM's) in spacecraft power sub-systems can exhibit unexpectedly severe SEE behaviours. SEE sensitivity in PWM's has also been the subject of recent NSREC papers (refs. iv and v). The European Space Agency has therefore sponsored a comprehensive investigation to characterise PWM SEE responses and to determine the source and cause of SEE sensitivity in these devices. A particular problem has been the difficulty in attributing an ion-induced SEE event to a particular function within the PWM circuit. Due to the feedback loops, which are inherent to these devices, SEE disturbances are propagated through various functional circuit blocks, such that it is difficult to determine where they originated. As a means of addressing this issue, two PWM device types have been probed with focussed, picosecond laser pulses using the Single Event Radiation Effects in Electronics Laser (SEREEL) facility at MBDA, Filton. The SEE responses for probing different areas of the microchip dies can be compared and matched with ion beam SEE responses, enabling ion SEE strike locations to be inferred.

5.1.2 The laser SEE investigation has also revealed new aspects of the SEE behaviour of PWM's, which are not directly apparent from ion beam tests. For example, the laser results have demonstrated that SEE sensitivity of PWM's varies in time through the output cycle as well as with position on the microchip die. The results indicate that there is enhanced SEE sensitivity when the output voltages are in the process of switching. Furthermore, a single-event latch-up (SEL) was found to have a significantly delayed onset relative to the laser pulse delivery time, when the laser pulse energy was close to the threshold for instigating the SEL.

5.2 Experimental details

5.2.1 Two Unitrode devices were investigated for this work: the UCC1806 low power, dual output, current mode PWM controller and the UC1825A high speed PWM controller. MBDA constructed a special interface circuit (Figure 5.1) in order to interface its test equipment with the test circuits designed by Saab Ericsson for the UCC1806 and UC1825A devices, which are shown in Figs. 5.3 and 5.5 respectively. In the case of the UCC1806, the relay steering inputs and Vrefin were all set at 5V for the laser testing. The UC1825A controlled a buck converter in voltage mode by tying the Ct and Ramp pins together. The ILIM/SD pin was grounded through a resistor. The buck converter ran in continuous mode and thus exhibited the characteristic damped resonance when controlled in voltage mode.

5.2.2 Heavy ion tests on both devices were performed by ESA and Saab Ericsson at the CYClotron of LOuvain la NEuve (CYCLONE) in Belgium. The high energy ion cocktail (M/Q = 3.33) was used in order to ensure a high penetration depth in Silicon (Table 5.3). The results are described in refs. ii and iii. Data on the ion SEE response of the closely related UC1806 device has also been available in ref. viii.

5.2.3 The laser SEE investigation consisted of probing of the exposed PWM dies with laser pulses at a large range of locations. The pulsed locations are identified in Figs. 5.2 and 5.4 for the UCC1806 and UC1825A respectively, together with the shot identifier numbers and the approximate equivalent LET threshold for upset (where calculable). The laser pulse energy could be varied continuously to establish the SEU or SEL threshold level at each location, which was found to exhibit SEE sensitivity. Traces from relevant device and circuit outputs were captured for each SEE event using digital oscilloscopes triggering on various of the outputs when they transgressed the limits of normal operation.

5.2.4 The triggering conditions utilised to detect SEE on the outputs were relatively sophisticated. Typically, window triggering modes were employed. For example, shot 22 on the UCC1806 utilised triggering for a duration on the OUTA pulse outside the range 400ns – 1200ns. The boundaries had to be relatively wide, because operational noise effects were otherwise found to induce triggering. The procedure was to widen the boundaries of the triggering range to the point where noise triggering without the laser pulses was inhibited, prior to the laser pulse testing. Triggering on the duration of the negative phase of the outputs and on transgression of an allowed window of noise range for Vref were also adopted in some cases. Triggering off the laser itself was not attempted, since it was usually necessary to deliver large numbers of pulses to test for upset thresholds. Triggering off the laser pulses with a further trigger condition on one or more PWM outputs would be optimal, but arranging for this is complex and was beyond the scope of the present work.

5.2.5 The conversions from laser pulse energy to LET were predicated on the comparison of laser and ion beam thresholds for the SRAM's tested in the first stage of this study (ref. i). This makes the absolute levels of LET somewhat uncertain, because the PWM's are a different technology (BICMOS) and the conversion factor is known to vary with technology and feature size. However the relative magnitudes of LET thresholds are expected to be more reliable.

5.3 Results

5.3.1 Lists summarising the outcomes of all laser shots that produced valid SEE responses are given in Tables 5.1, 5.2 and 5.4. Some other laser pulse locations did not produce a response up to the maximum pulse energy that could be delivered without changing the fixed filtration (which would have required a recalibration). Some of these locations are indicated with magenta spots in Figure 5.4, for example. A further problem was that the cable on the Error Amplifier output for the UC1825A was found to be picking up EMC noise from the laser. This rendered shots 1 to 17 for the UC1825A problematic, but the problem was cured by removing the Error Amplifier cable from shot 18 onwards.

5.3.2 Examples of output traces for the UCC1806 device are shown in Figures 5.6 to 5.12. Figure 5.6 shows an SET for a pulse delivered amongst a dense area of circuitry on the microchip die adjacent to the CURLIM bond wire pad. Around four output pulses were lost. The upset appears on all the outputs virtually simultaneously, so it would prove difficult to guess the location of an equivalent upset seen in ion beam testing. Figure 5.7 shows a SET, which gave a series of short output pulses for a delivery location in a dense area of circuitry between the CT, RT and central GND bond wire pads. The upset scarcely appears on the EAOUT and VREF outputs, so it may be a timing circuit (frequency setting) issue. In Figure 5.8, the upset was induced in a part of the die very close to the AOUT bond wire pad and it is clear from the traces that it is the AOUT output that is affected earliest. A lowering of the first AOUT pulse after the upset was seen, which did not occur in any other shot location. Figure 5.9 shows a SET for shot 35 not far from shot 12 (Figure 5.6) on the die. It had a lower threshold than for shot 12 and the effects were similar in overall nature, but less prolonged and lower in magnitude.

5.3.3 Figures 5.10 to 5.12 show the captured responses for latchup events (SEL). Actual latchup seems to have been delayed relative to the appertaining SET in the case of shot 51 (Figure 5.10). However the characteristic latchup current of 100mA appeared on the Vstart 9-10V line. The delayed onset of the laser induced SEL near its pulse energy threshold was confirmed by the results shown in Figure 5.12 (shot 56): the device first suffers an SET, from which it starts to recover 10μs later, but SEL cuts in at 20μs after the instigating event. However, the SEL was immediate well above the threshold pulse energy (Figure 5.11, shot 55). This SEL was encountered within a single region a few micrometers square of the UCC1806 die as indicated in Fig. 5.13. Note that the lowest SEL threshold (5.7 MeV cm^2/mg) was only seen once (shot 51) and was not repeatable. The threshold in repeatable testing was 63 MeV cm^2/mg (shot 56). The lower unrepeatable threshold may have had a very narrow time window in the operational cycle and/or an extremely small spatial cross-section. This probably explains why latch-up was not seen in the ion testing: the SEL cross-section is likely to be vanishingly small below 63 MeV cm^2/mg, which level is above the LET range for the ion beam testing (Table 3).

5.3.4 Examples of output traces for the UC1825A device are shown in Figures 5.14 to 5.24. Figure 5.14 shows an example of an upset observed when the EAOUT cable was picking up emc interference. The combination of long and short pulses with missing pulses in two ranges is not too different in form to genuine laser-induced SET's. Unfortunately, however, emc induced events were also seen with the laser shutter closed, so these results (up to shot 17) cannot be trusted.

5.3.5 The laser induced SET's seen for the UC1825A were very variable in severity, ranging from very slight pulse width changes (e.g. Figure 5.21) through to severe upsets with significant transient voltage reductions on the output (e.g. Figures 5.16, 5.19 and 5.22). Note however that Saab Ericsson have attributed the long recovery time of some of the severe events to capacitance in the cables. Some of the SET's appeared to exhibit low thresholds. Certainly, the UC1825A showed events with laser pulse energy thresholds much lower than was seen in the UCC1806. The equivalent threshold LET's ranged down to 0.2 MeV cm^2/mg for the UC1825A, but only to 1.6 MeV cm^2/mg for the UCC1806.

5.3.6 The output traces for ion and laser Single Event Transients (SET's) can be compared. Three ion-induced SET's from the Saab-Ericsson results are shown in Figures 5.25 to 5.27. As a case study consider the SOFTSTART traces in Figures 5.17, 5.20 and 5.23. Note that the SOFTSTART voltage sinks steeply and instantly for laser shots 23 and 33 and also for the ion SET's in Figures 5.25 and 5.27. These laser shots were delivered in the vicinity of the NI and INV bond wire pads. Conversely, there is a delay of a few pulse widths after the SET begins before the SOFTSTART voltage plunges for laser shot 38 and also for ion beam SET #71-3 (Figure 5.26). This laser shot was located near the SOFTSTART and ILIM/SD bond wire pads on the PWM die. The different responses of the SOFTSTART output may therefore be associated with ion strikes on different areas of the die with reference to the laser SEE test results. (Note also that the voltage reference VREF was unaffected in all cases.)

5.3.7 The laser investigations revealed variations in SEE sensitivity across the die that were pronounced and which occurred on a fine spatial scale. Many locations were found to be SEE insensitive, whilst the SET threshold pulse energies varied by several orders of magnitude among those sites that were found to be susceptible. Typically, both the form of a SET and its energy threshold were found to vary significantly on a scale of micrometers everywhere.

5.3.8 It was found that a proportion of SET sensitive locations on the PWM dies typically only produced a SET response for one in tens of laser pulses delivered. Some of the shots for which this effect was particularly evident are identified in the "comments" column of Tables 5.1, 5.2 and 5.4. Although the laser pulses vary slightly in energy from shot to shot, a SET was sometimes still only seen for one in tens of pulses at pulse energies well above the threshold. Since the energy of all pulses would have been above the SET threshold in these cases, the only likely explanation is that the SET sensitivity was only exhibited during transitory periods of the operational cycles of the PWM's. The low proportion of shots that gave rise to SEE's in these cases is most consistent with enhanced SEE sensitivity during switching of the output voltages. Note that a high proportion of the SET's shown in Figures 5.6-5.12 and 5.15-5.27 appear to have occurred on rising or falling edges of the output pulse trains.

5.4 Conclusions

5.4.1 The laser investigation of the PWM's has revealed an extremely complex range of behaviour. The SET cross section appears to vary through the output cycle as well as spatially across the die. The form of the SET's is also highly variable in duration, magnitude and general severity. It has been shown that the laser provides a means of associating upsets with particular locations on the die. The laser testing has illuminated the heightened SET sensitivity when the output voltage is switching. The laser has also demonstrated its special propensity for discovering latchup sensitive locations.

5.4.2 It should be possible with the new SEREEL laser facility to conduct a more comprehensive survey of the SEE sensitivity of the PWM dies. It would be necessary to deliver a grid of laser pulses across the dies at a range of threshold energies and under computer control. Use of different wavelengths could also be employed to investigate variations in SEE sensitivity with depth into the silicon of the dies. This would also require triggering off the laser pulses and storage of pulse traces subject to a further trigger condition on a suitable PWM output signal. Such a survey would enable the expression of the laser results in more rigorously quantitative terms.

Table 5.1. UCC1806 Laser Pulses (Sample 1)

Shot Number	Equiv. LET	Threshold	Lost Pulses	Comments
5	254	N	~3	
6	130	N	0	Minor effects
7	77	Y	0	Minor effects
8	425	N	~3	
9	254	Y	0	Minor effects
10	380	Y	0	Minor effects
11	44	N	~3	
12	42	Y	~4	
13	800	Y	~2	After many pulses
14	44	N	1	
15	8.8	Y	Short pulse	
16	130	N	1	
17	800	Y	0	Slightly short pulse?
18	23	Y	0	Negative spike in pulse
19	130	N	~1	
20	425	?	>>6	Intermittent/unrepeatable
21	425	?	>10	Intermittent/unrepeatable
22	425	N	0	Small spike in pulse
23	254	Y	0	Slightly short pulse?
24	2.32	Y	0	Minor effects
25	7.5	N	Short pulse	
26	21	N	Short pulse	
27	44	Y	0	Conjoined pulses
28	44	Y	V. Short pulse	After many pulses
29	225	N	0	Several short pulses
30	15	Y	0	Conjoined pulses
31	80	N	~1	
32	20.5	Y	0	Minor effects
33	225	N	0	Minor effects
34	29	Y	0	Minor effects
35	1.8	Y	1	
36	7.5	N	1	
37	10.4	Y	~2	
38	35	N	~2	
39	19.5	Y	0	Minor effects
40	35	N	1	
41	10	N	0	Minor effects
42	7.5	N	0	After many pulses
43	4.1	Y	0	With position nudge

Table 5.2. UCC1806 Laser Pulses (Sample 2)

Shot Number	Equiv. LET	Threshold	Lost Pulses	Comments
44	43.9	N	0	Minor effects
45	27.7	Y	1	
46	27.7	N	1	And a short pulse
47	2.47	N	1	
48	2.47	N	2	
49	1.6	Y	0	Minor effects
50	145	N	1 & 1	Good pulse between
51	5.7	Y	1	Delayed latchup, unrepeatable
52	44	N	(2)	Merged pulses
53	11	Y	(1)	100 pulses to upset
54	26	N	1	Upset only – no latchup
55	460	N	-	Immediate latchup
56	63	Y	1	Latchup after delay

Table 5.3. Heavy Ions Used At CYCLONE

ELEMENT	ENERGY [MeV]	RANGE (Si) [μm]	LET (Si) [MeV cm^2/mg]
Ne-20	235	199	3.33
Ar-40	372	119	10.9
Kr-84	756	92	32.4

Table 5.4. UC1825A Laser Pulses

Shot Number	Equiv. LET	Threshold	Lost Pulses	Comments
18	8.36	N	1	
19	6.64	Y	~1	Long & short pulses
20	47	N	0	Long & short pulses
21	2.2	N	>7 (2 groups)	Threshold ~10x lower
22	0.35	N	>8	In 2+ groups
23	0.31	Y	>7	In 2+ groups
24	11.7	Y	0	Slightly long/short
25	11.7	Y	0	Slightly long/short
26	20	Y	0	Spike in trough
27	1.85	Y	0	Short pulse
28	1.85	Y	0	Long & short pulses
29	16.4	N	0	Long & short pulses
30	3.9	Y	0	Long & short pulses
31	20	N	0	Long & short pulses
32	11	N	>8	In 2+ groups
33	4.65	Y	>7	In 2+ groups
34	0.7	Y	0	Long & short pulses
35	16.4	N	1 & 1	Good pulse between
36	3.3	Y	Short pulse	Minor effects
37	0.42	Y	>8	In 2+ groups
38	0.42	Y	>7	In 2+ groups, many pulses required
39	1.08	N	~8	In 2 groups
40	3.7	Y	0	Short gap
41	0.2	Y	1	
42	0.35	N	0	Short gap
43	20	N	~0	Long/short (severe)
44	10.4	Y	0	Slightly long/short

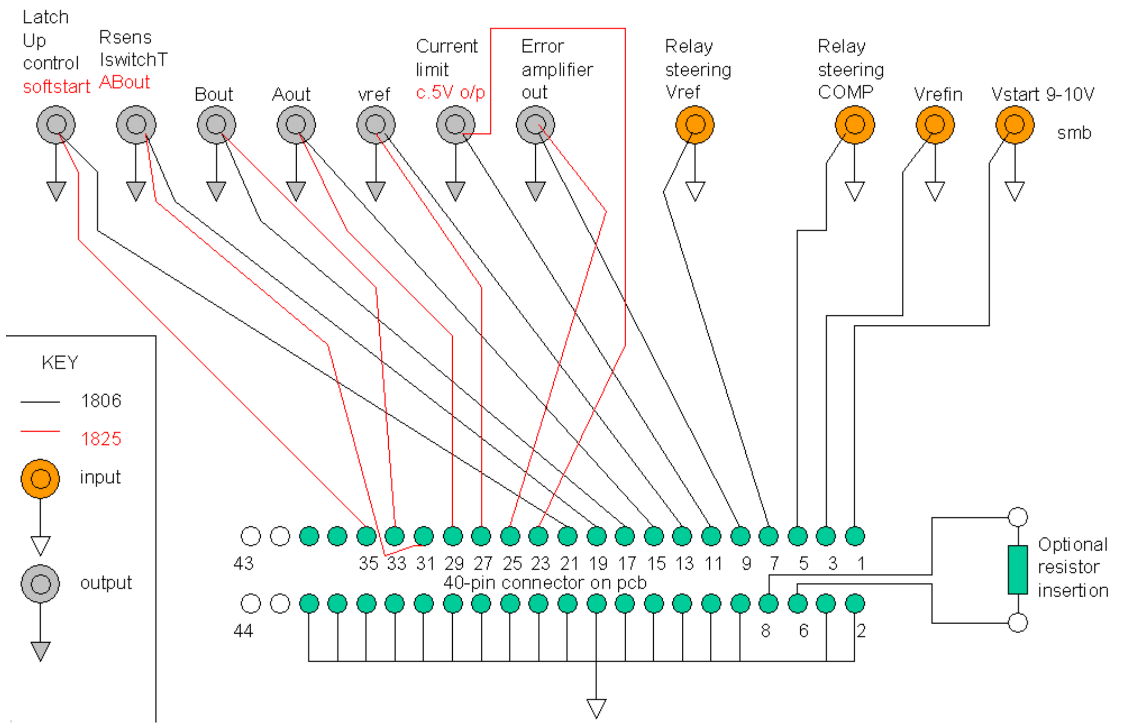

Figure 5.1. Interface card between the PWM PCB and support equipment.

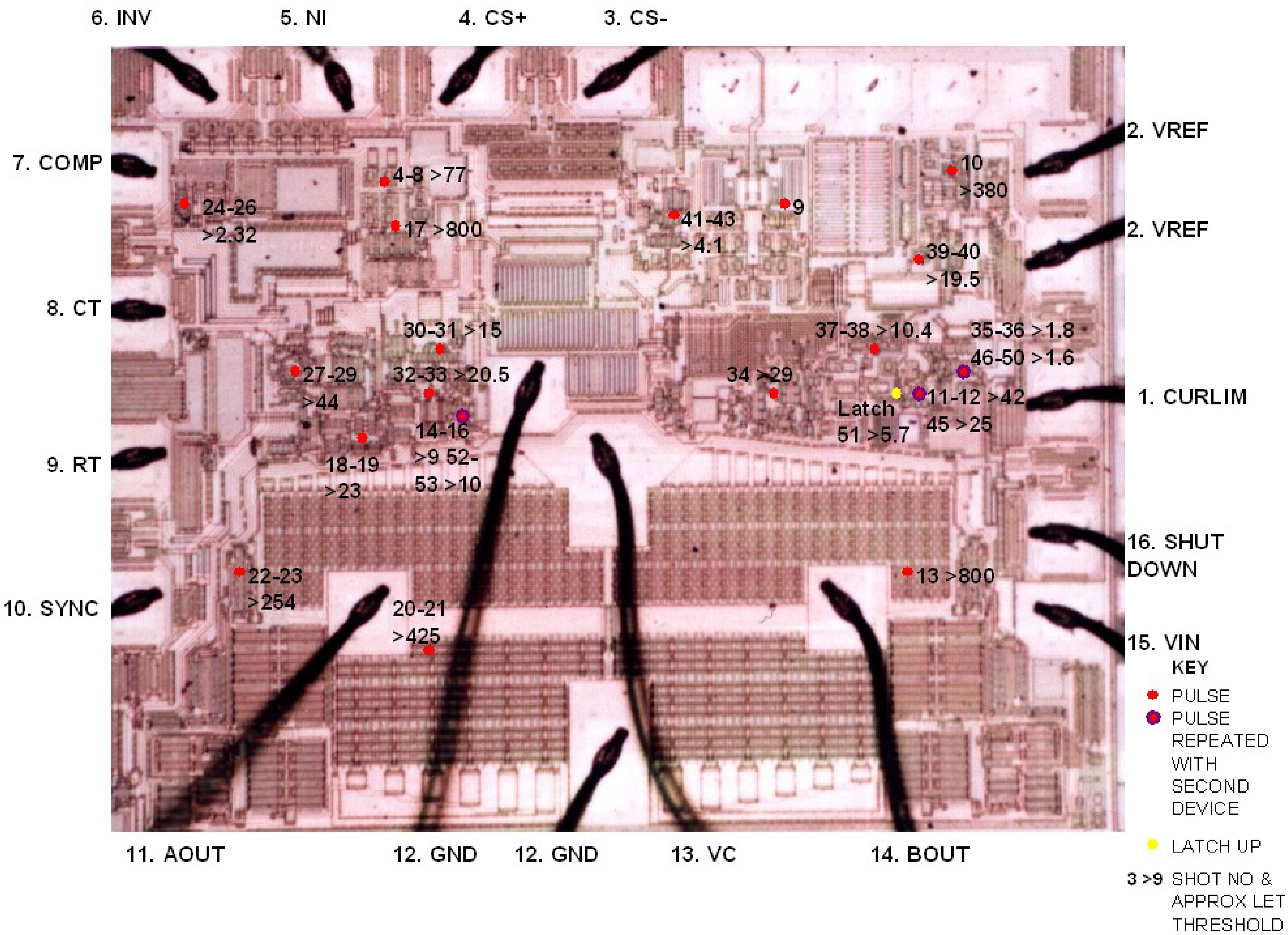

Figure 5.2. Image of the UCC1806 Pulse Width Modulator microchip die.

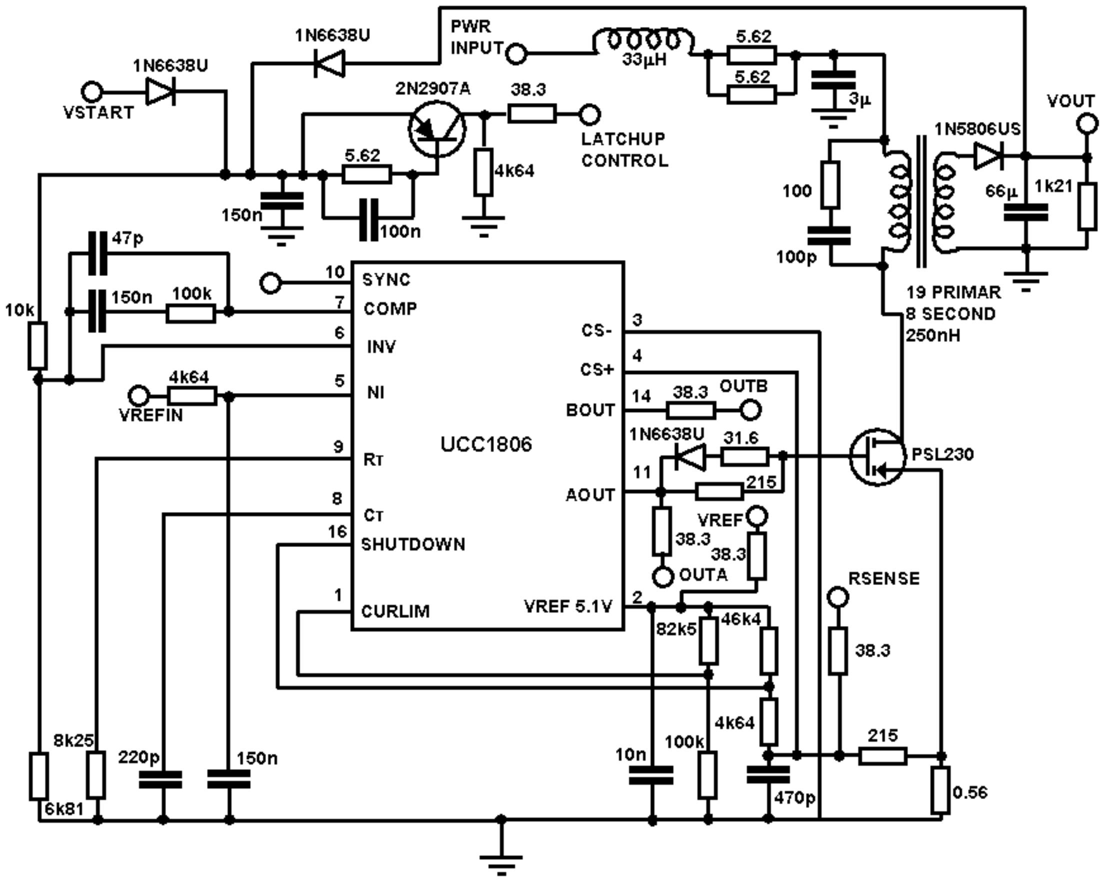

Figure 5.3. The UCC1806 test circuit.

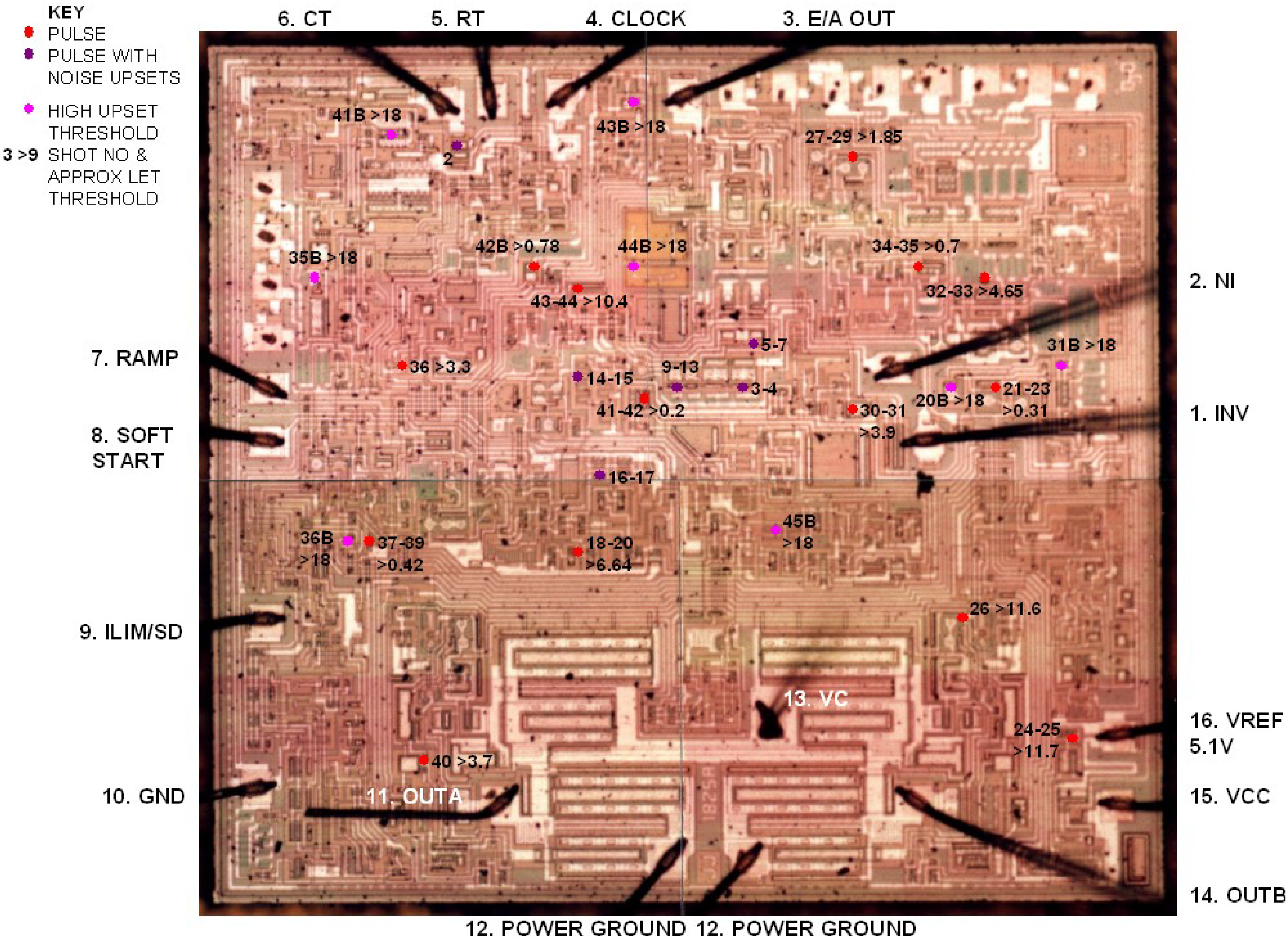

Figure 5.4. Image of the UC1825A Pulse Width Modulator microchip die.

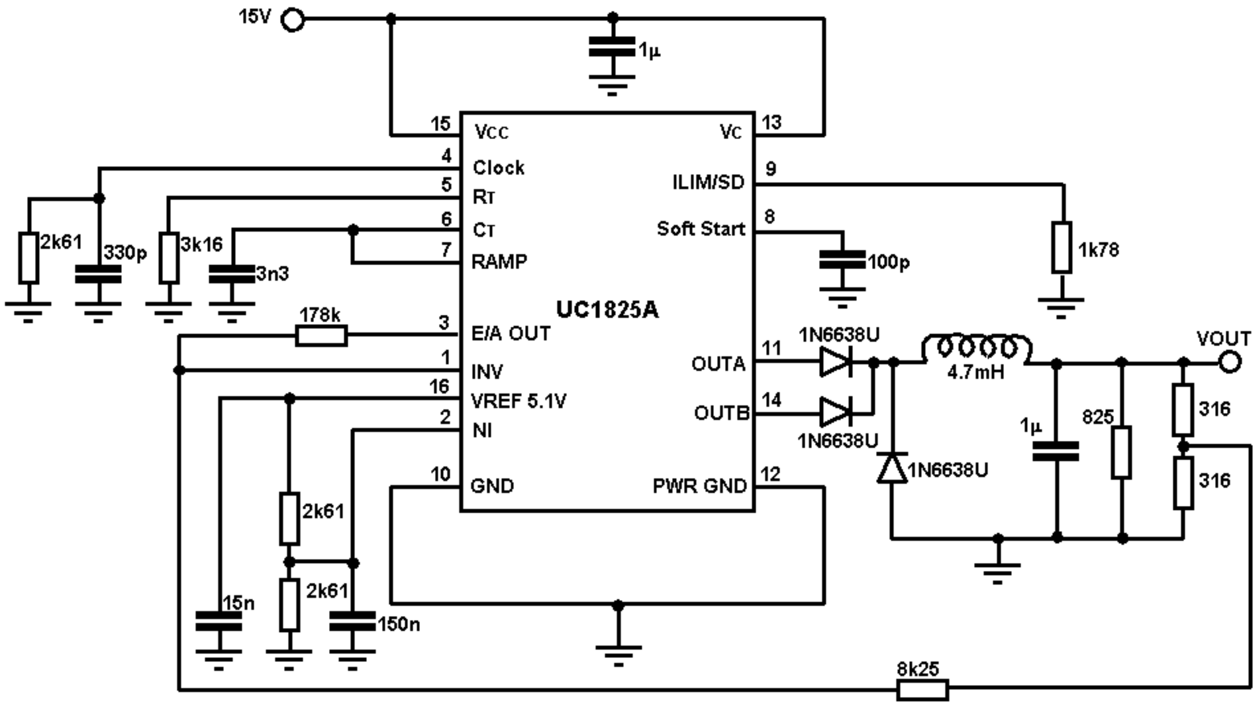

Figure 5.5. The UC1825A test circuit.

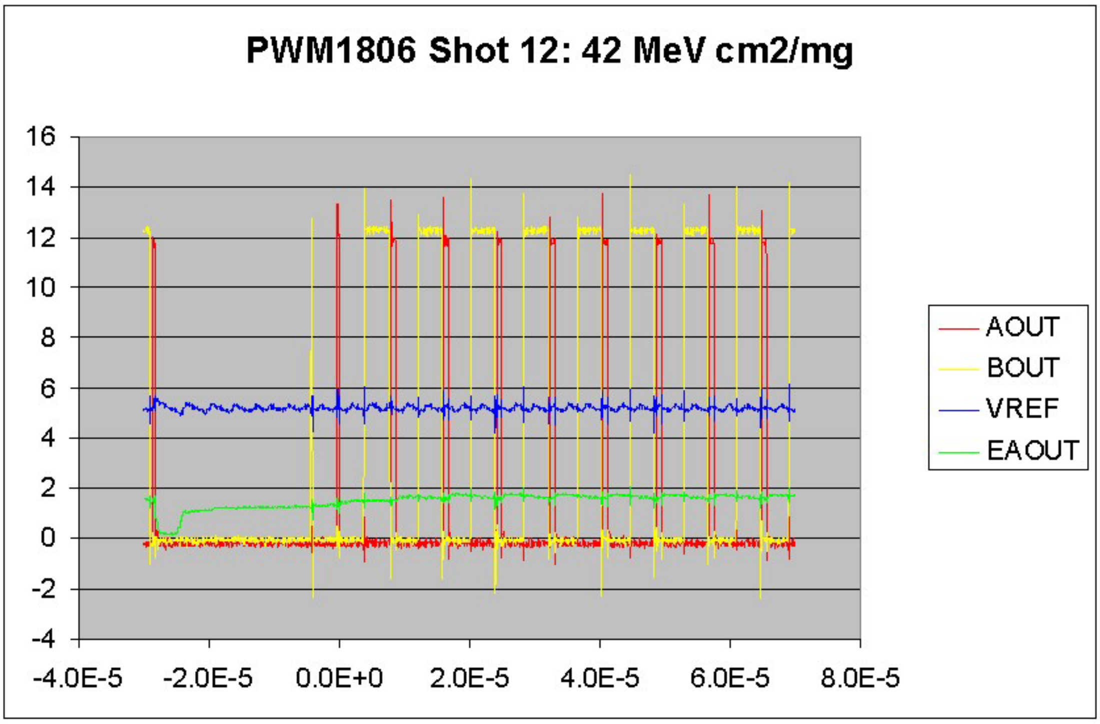

Figure 5.6. Laser induced SET near the CURLIM bond wire pad of the UCC1806

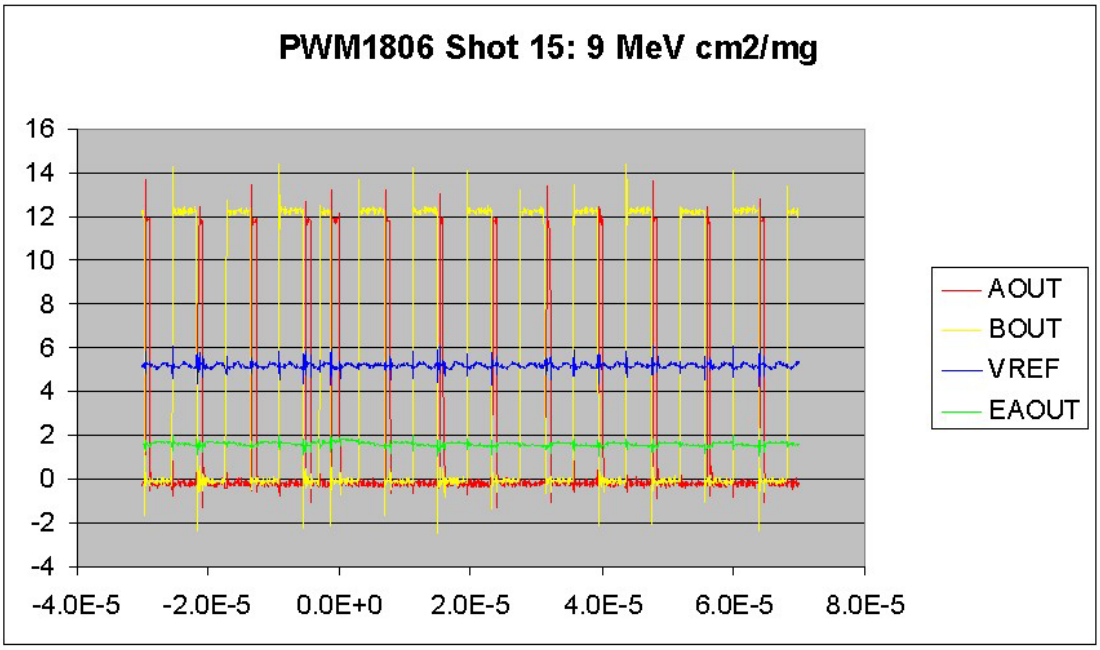

Figure 5.7. Laser induced SET near the central GND bond wire pad of the UCC1806

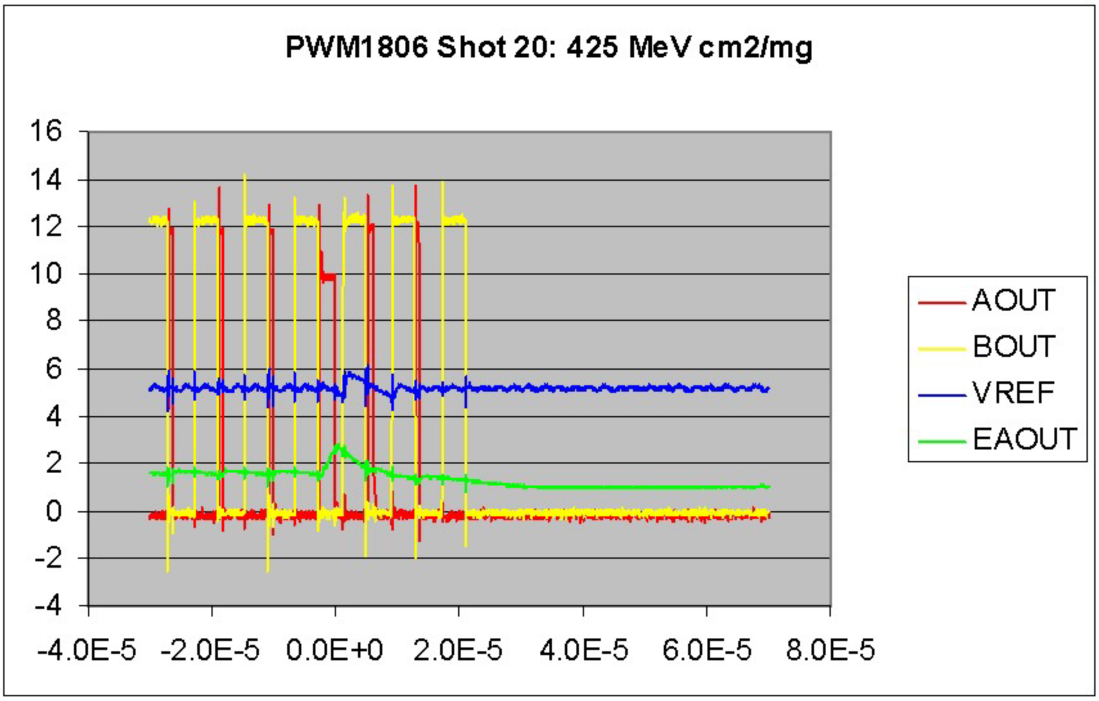

Figure 5.8. Laser induced SET near the AOUT bond wire pad of the UCC1806

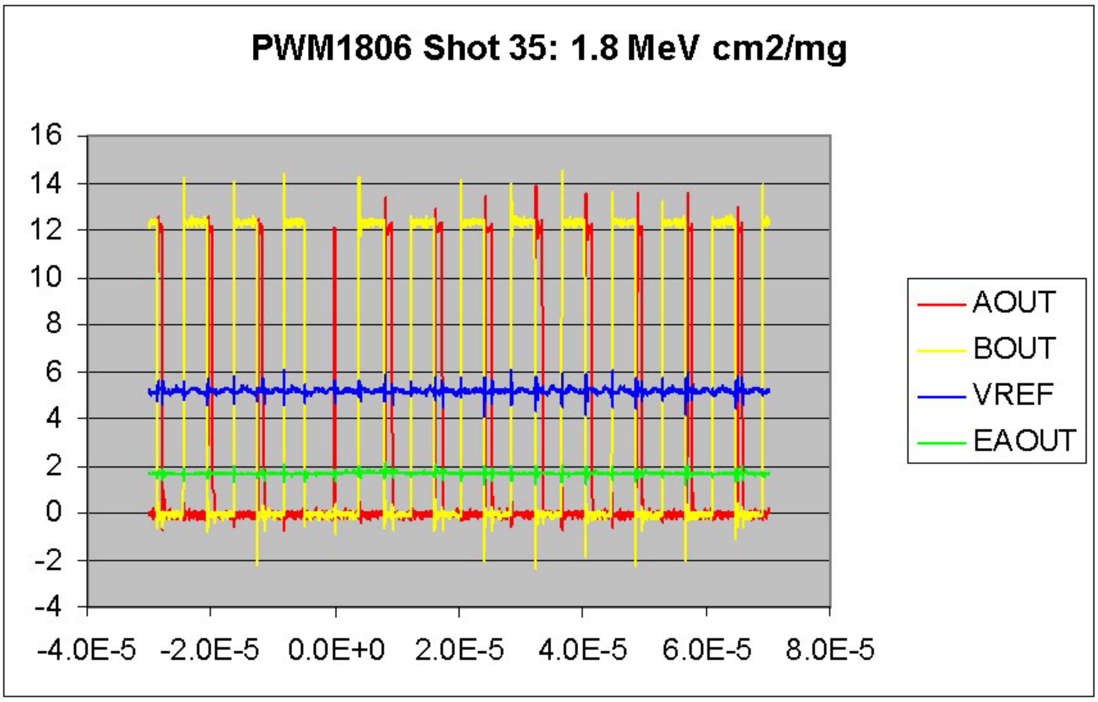

Figure 5.9. Laser induced SET near the CURLIM bond wire pad of the UCC1806

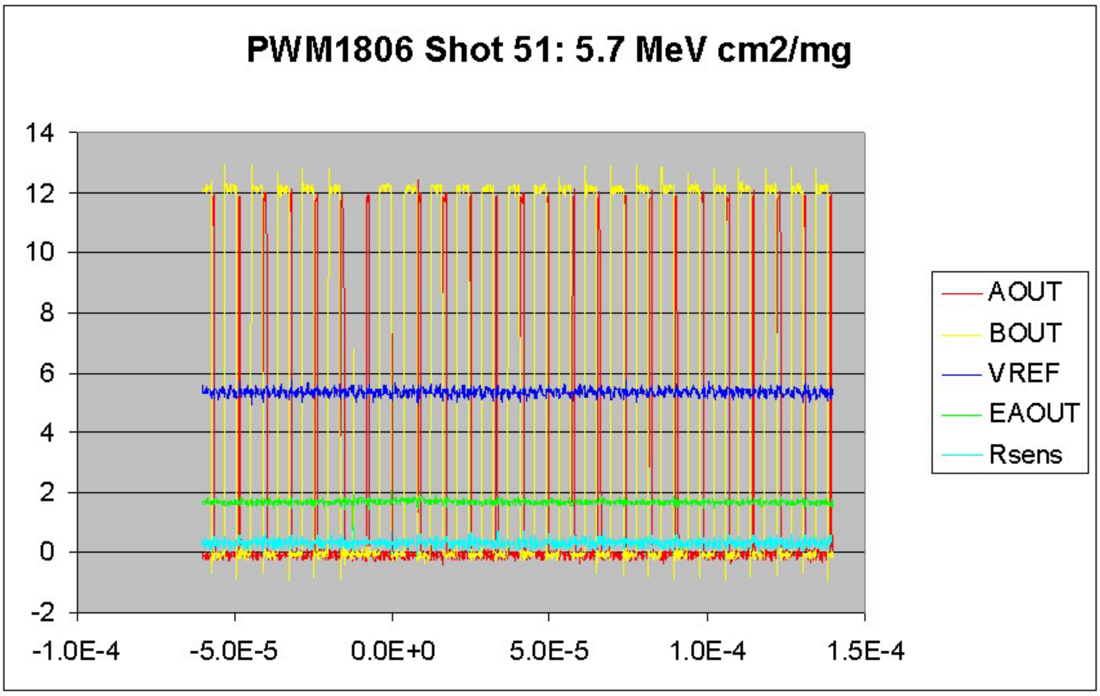

Figure 5.10. SET preceding delayed latchup of the UCC1806

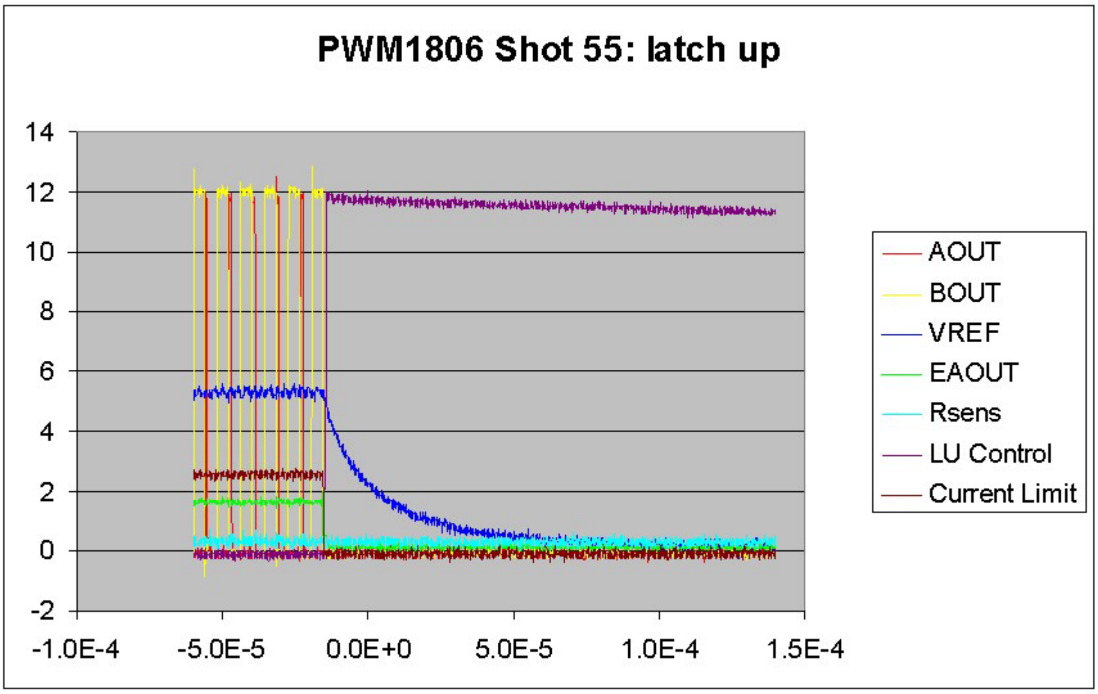

Figure 5.11. Immediate latchup of the UCC1806

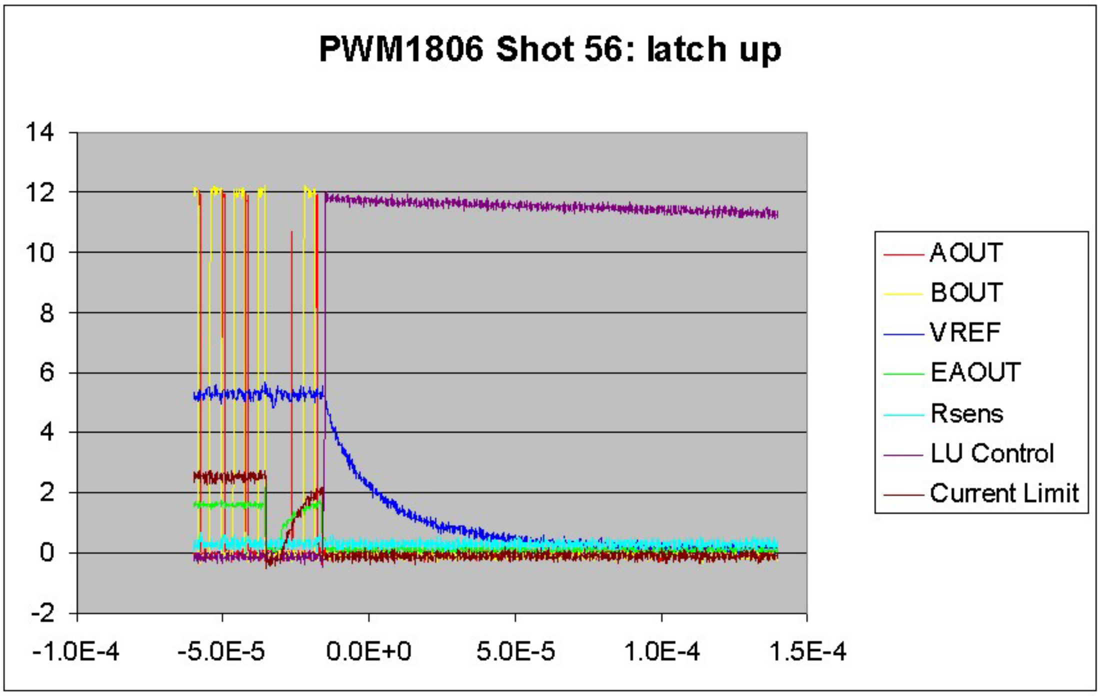

Figure 5.12. SET and delayed latchup of the UCC1806

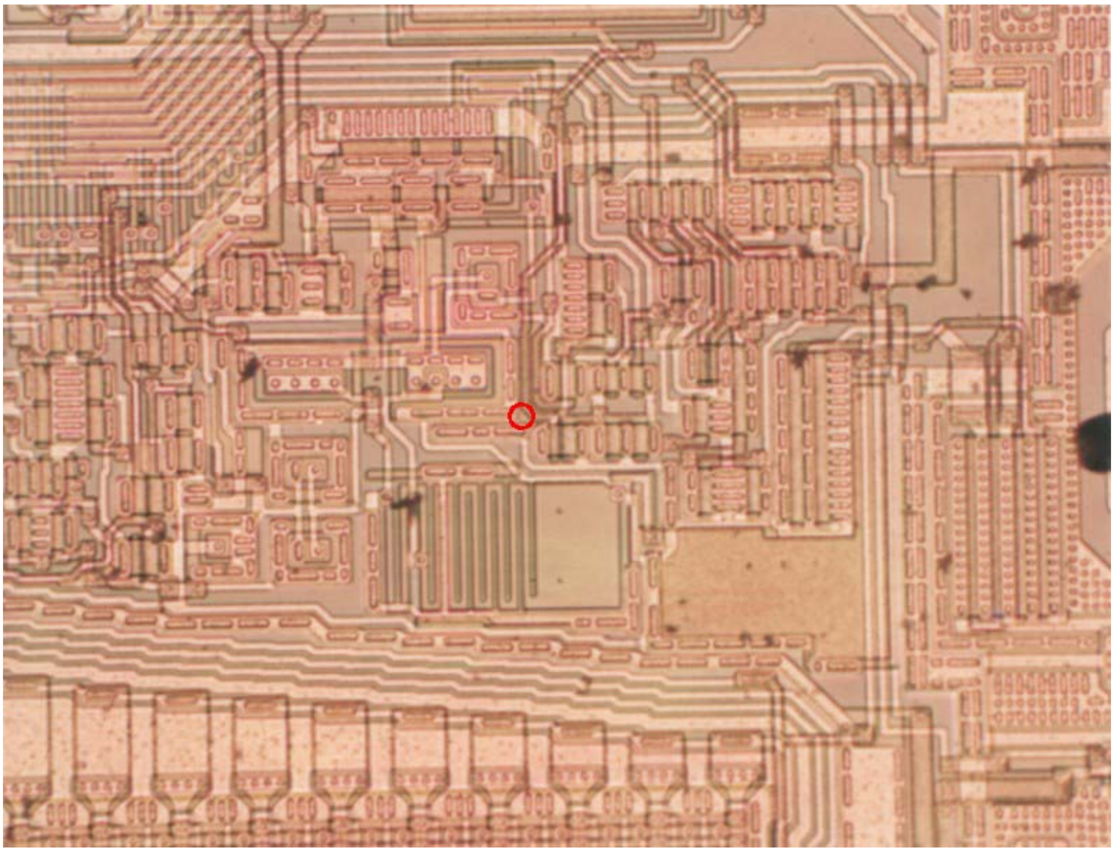

Figure 5.13. Site of SEL sensitivity on the UCC1806 die

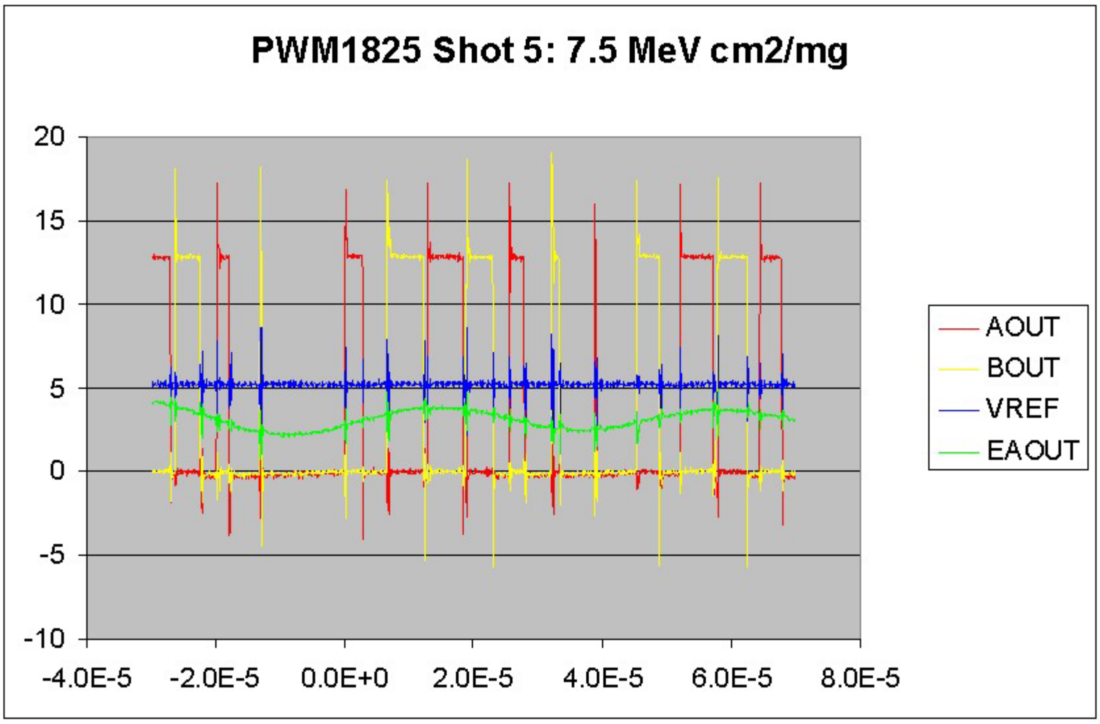

Figure 5.14. SET in the UC1825A for the EAOUT lead attached

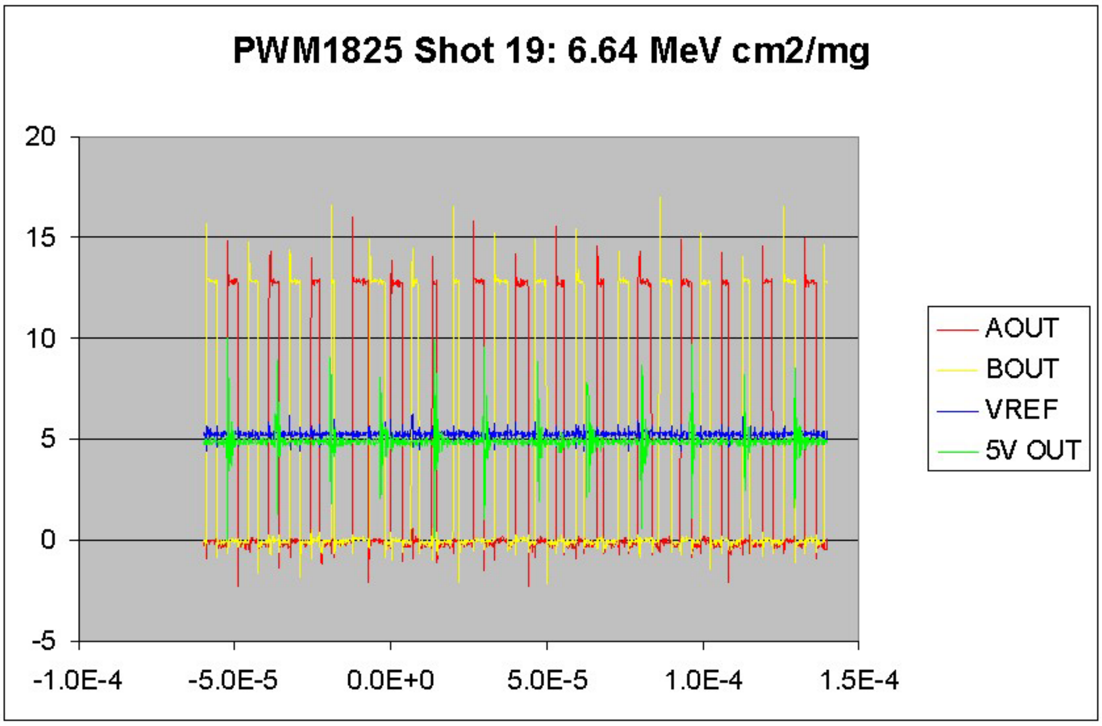

Figure 5.15. SET in the UC1825A for a pulse location near the middle of the die.

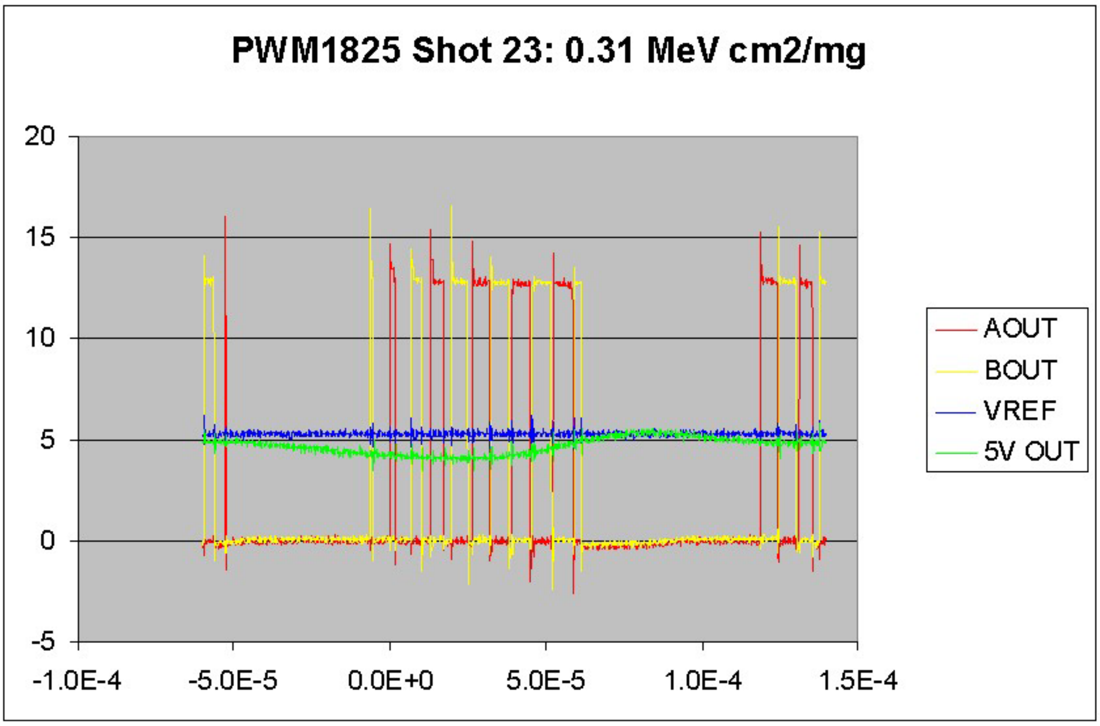

Figure 5.16. SET in the UC1825A for a pulse location near the NI and INV (error amplifier) bond wire pads

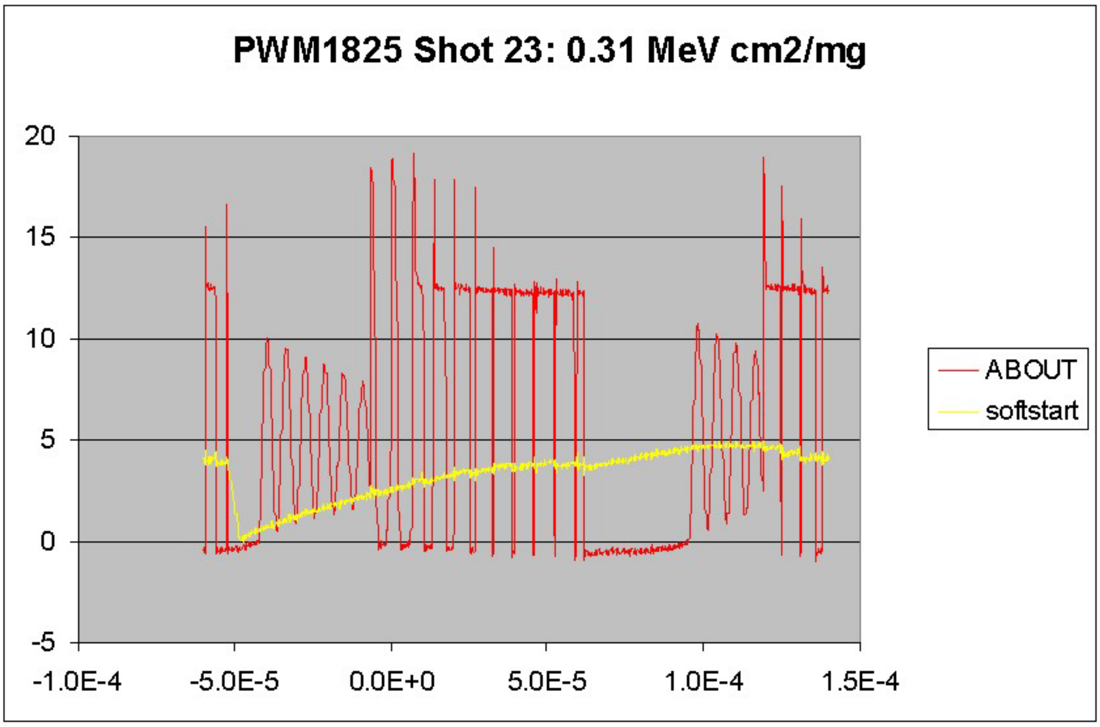

Figure 5.17. SET in the UC1825A for a pulse location near the NI and INV (error amplifier) bond wire pads (continued)

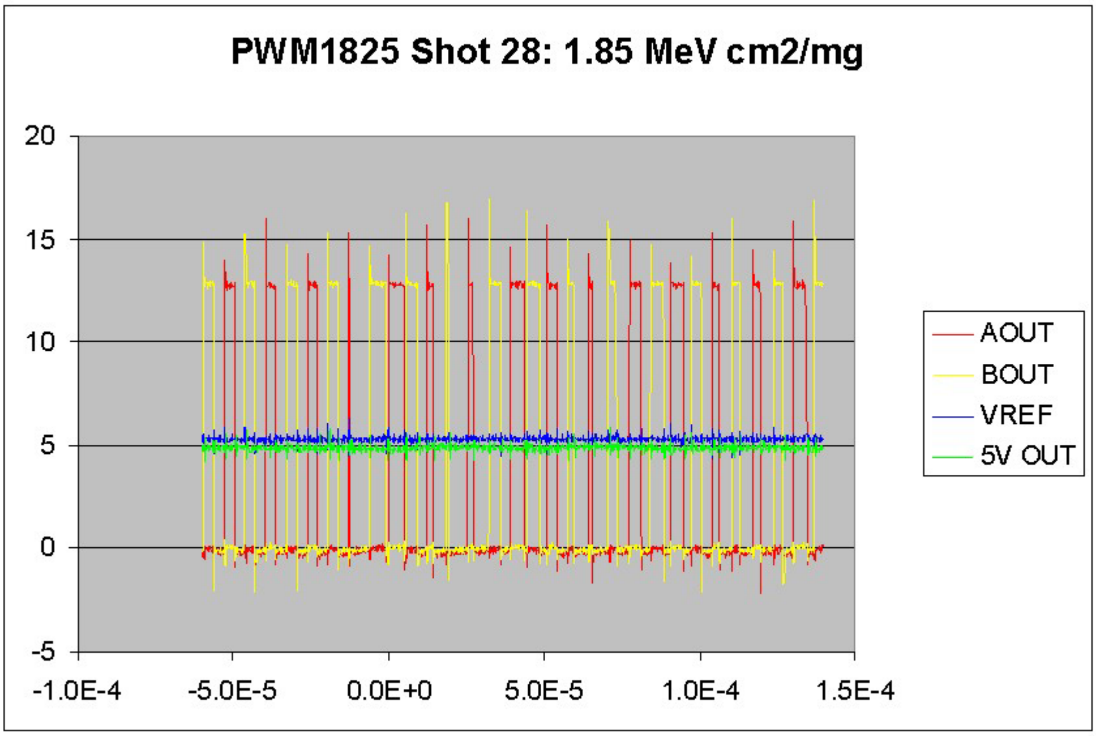

Figure 5.18 SET in the UC1825A for a pulse location between the NI and EAOUT bond wire pads

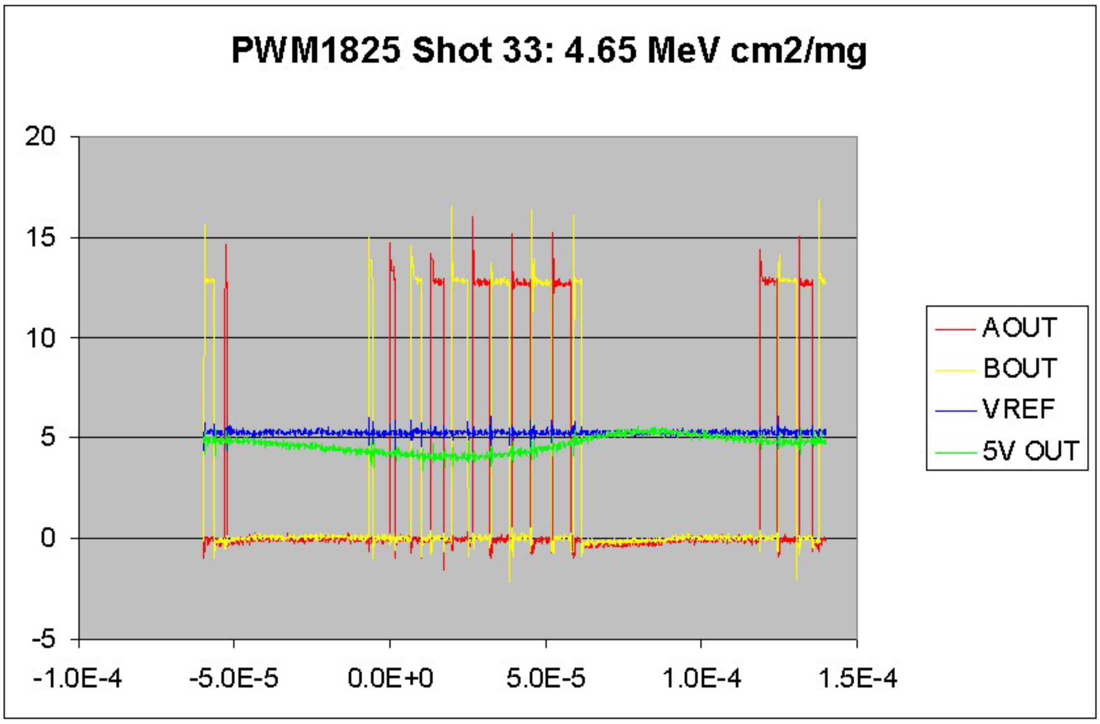

Figure 5.19. SET in the UC1825A for a pulse location near the NI bond wire pad

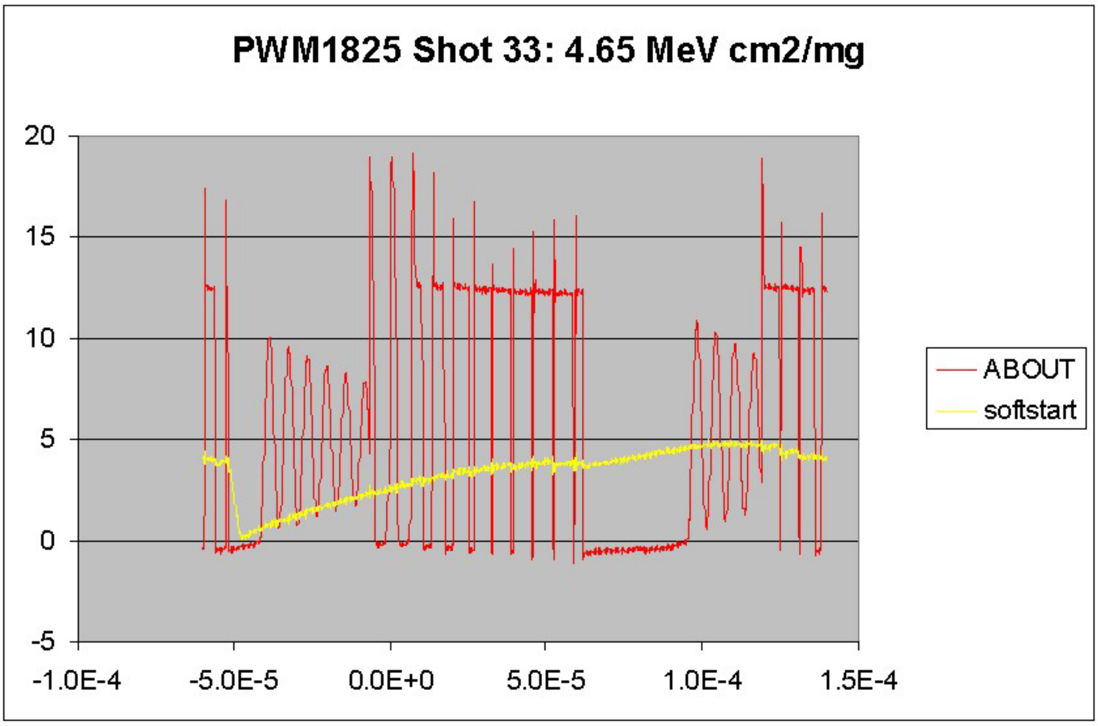

Figure 5.20. SET in the UC1825A for a pulse location near the NI bond wire pad (continued)

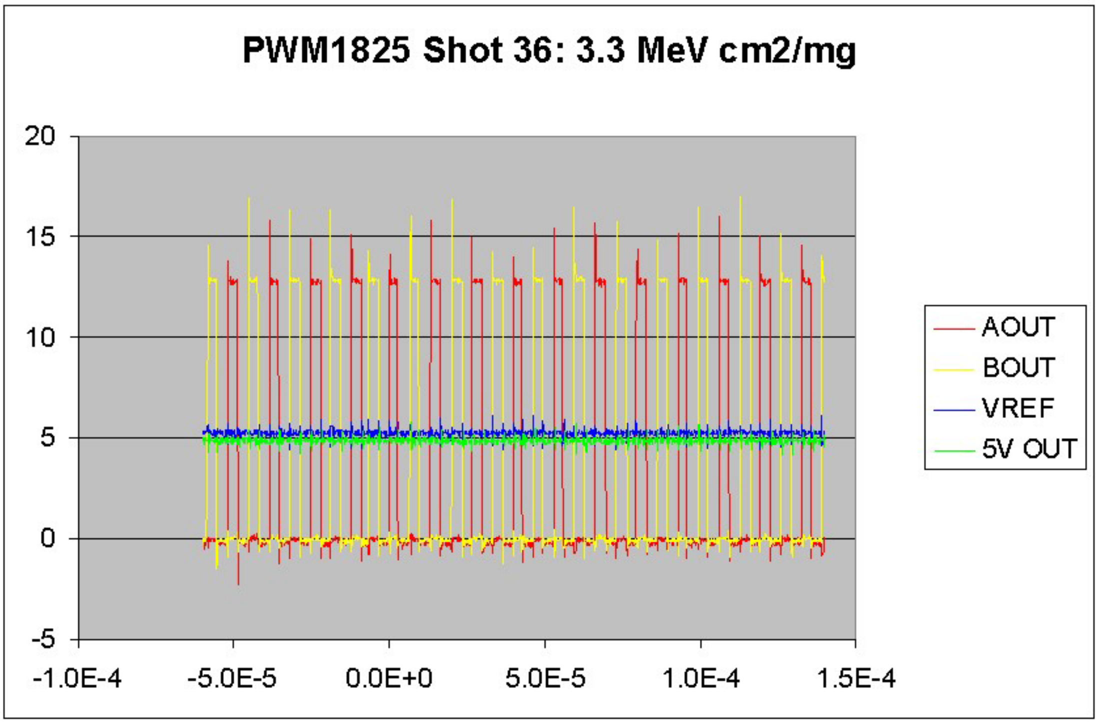

Figure 5.21. SET in the UC1825A for a pulse location near the RAMP and SOFTSTART bond wire pads

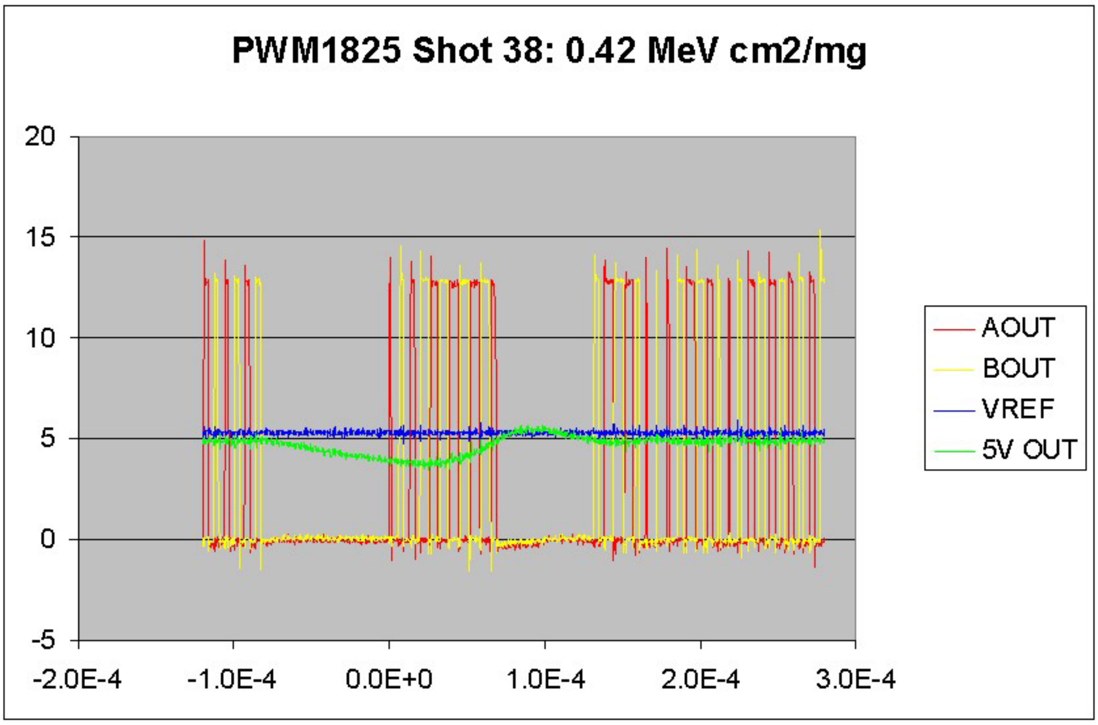

Figure 5.22. SET in the UC1825A for a pulse location between the SOFTSTART and ILIM/SD bond wire pads

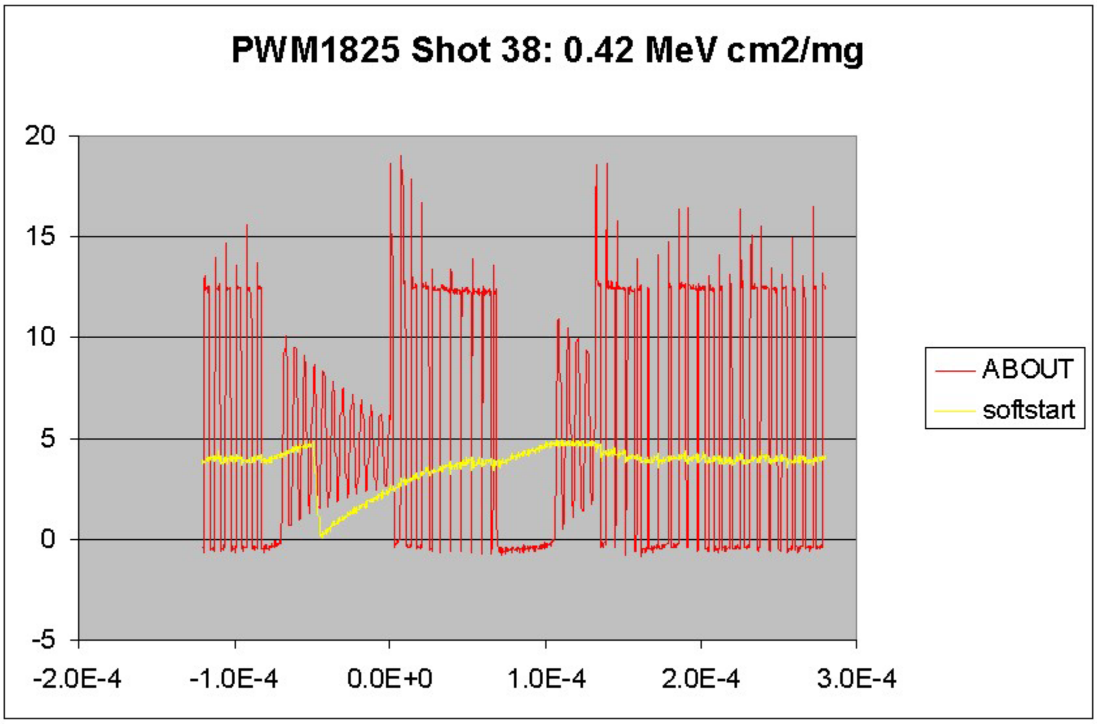

Figure 5.23. SET in the UC1825A for a pulse location between the SOFTSTART and ILIM/SD bond wire pads (continued)

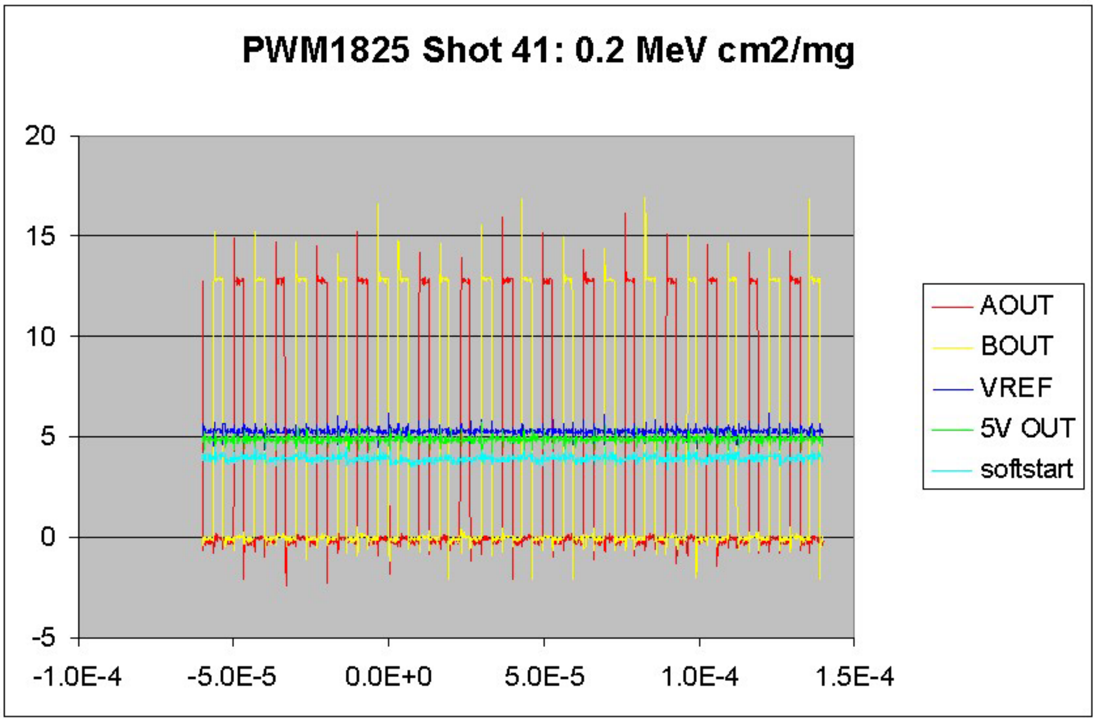

Figure 5.24. SET in the UC1825A for a pulse location in the central region of the die

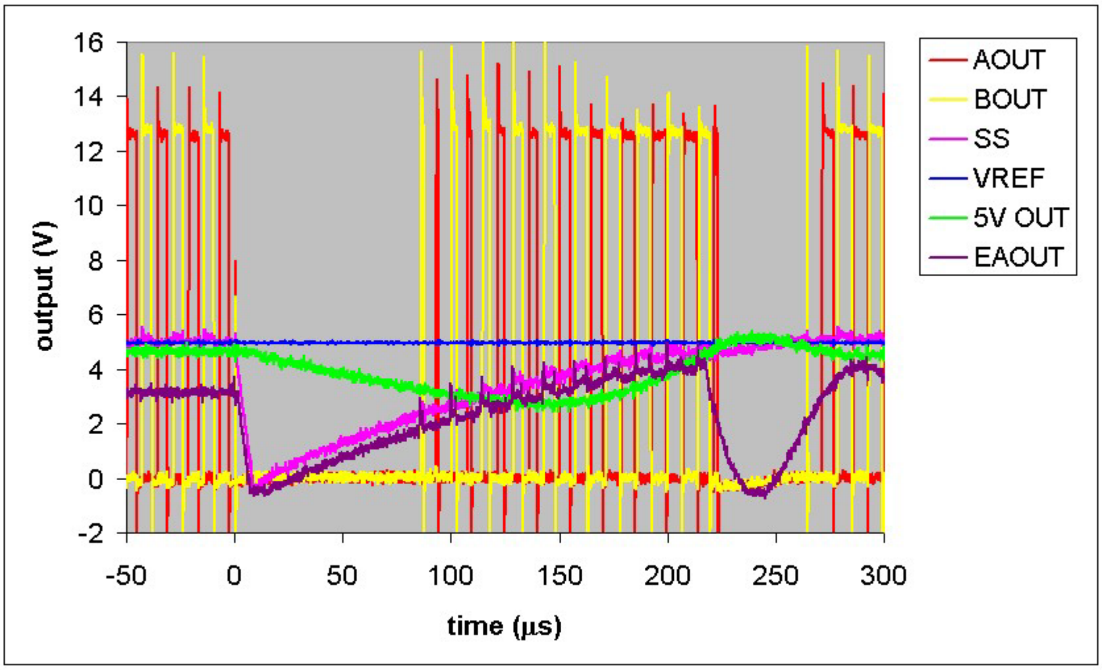

Figure 5.25. Ion beam SET in the UC1825A (run #64-1)

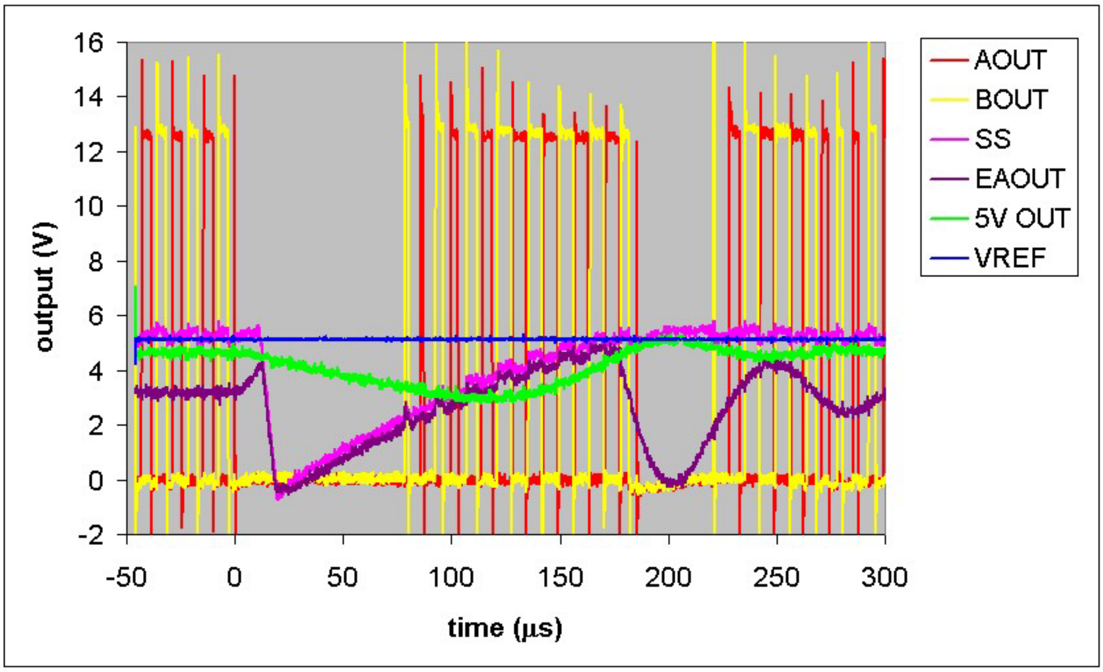

Figure 5.26. Ion beam SET in the UC1825A (run #71-3)

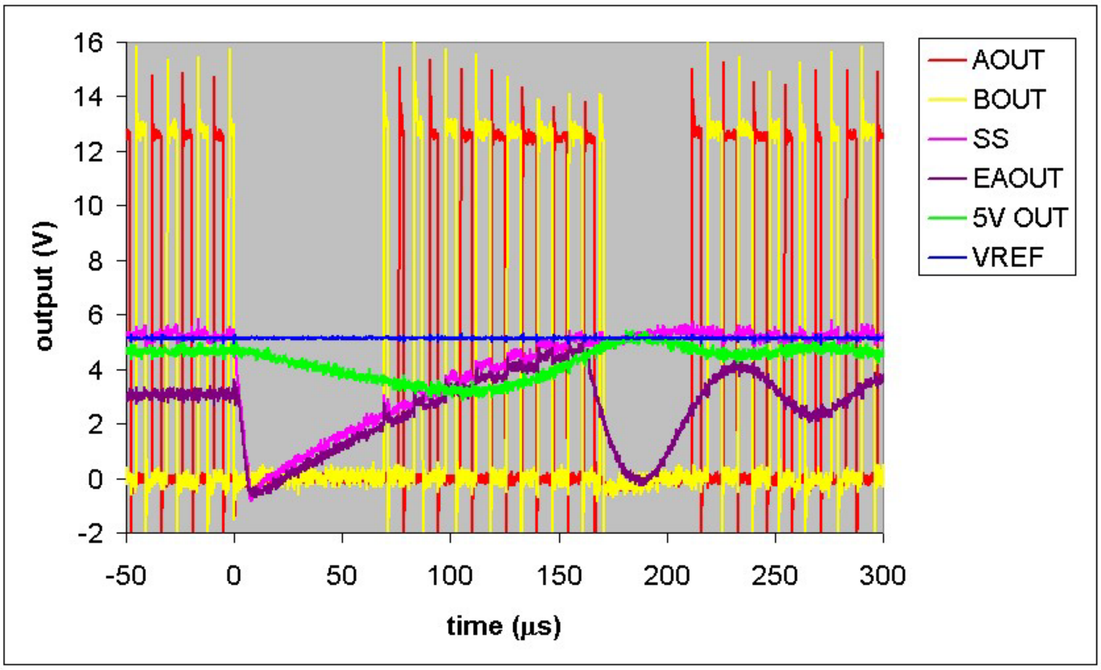

Figure 5.27. Ion beam SET in the UC1825A (run #72-25)

6 THE SEREEL2 LASER FACILITY

6.1 Specification and Ordering

6.1.1 In 2003 MBDA began planning the replacement of the SEREEL laser SEE test facility with a new, more powerful and commercially oriented successor facility, known as SEREEL2 (figure 6.1). In 2005, these plans have been brought to fruition with the specification, selection and funding of a new laser for the SEREEL2 facility (Figure 6.2). The new laser will be computer controlled (Figure 6.3), replacing complex and time-consuming manual adjustments for the existing system. The new laser is capable of delivering a continuous range of optical and infrared wavelengths under computer control (Figure 6.4), thus considerably enhancing the capability of the system to probe for SEE sensitivity at varying depths into the silicon.

6.1.2 The order for the new laser was placed on 14th December 2004. There is a 4 month lead time on delivery, so the laser will not enter service until around May 2005. However, several elements of the new SEREEL2 facility have already been implemented in the existing SEREEL facility in the course of the last year (Figure 6). The new features include a) the pulse energy CCD camera on the 3-axis positioning system, b) the adjustable pulse attenuator and c) the manual part of the positioning system. These items are operating well and have been applied successfully to the work reported here.

6.2 Enhanced Capabilities

6.2.1 The new laser SEE test system will be a far more flexible and powerful investigative tool that the old system. Whereas SEREEL1 was primarily a research apparatus, SEREEL2 has been designed for ease of use combined with accuracy and repeatability. It will greatly enhance the capabilities of the Radiation Effects Group in respect of SEE investigations. Further improvements are planned for 2006: in particular a new microscope will be acquired with higher magnification objectives in order to compensate for the ongoing shrinkage of feature size.

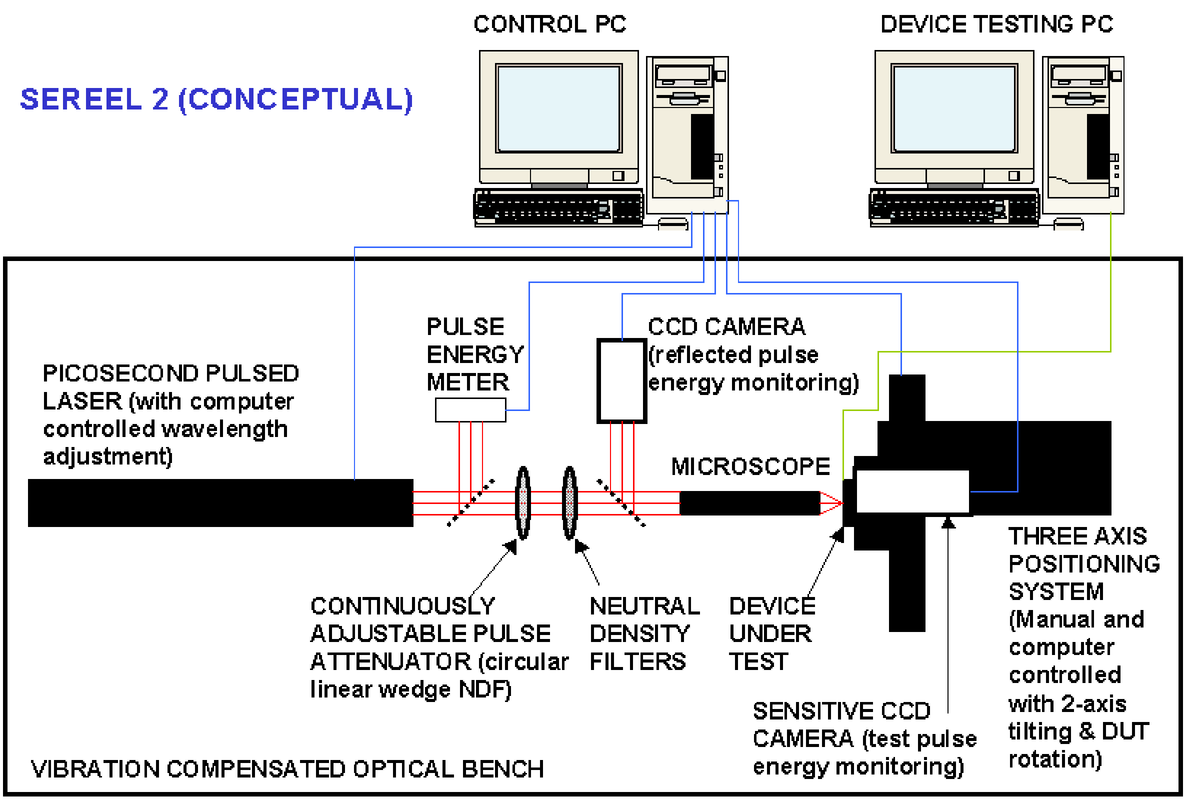

Figure 6.1. SEREEL 2: the pulse energy CCD camera on the 3-axis positioning system, the adjustable pulse attenuator and the positioning system have already been implemented and have been used for this contract. The new laser is scheduled for Spring 2005.

Figure 6.2. The new laser and the optical parametric amplifier

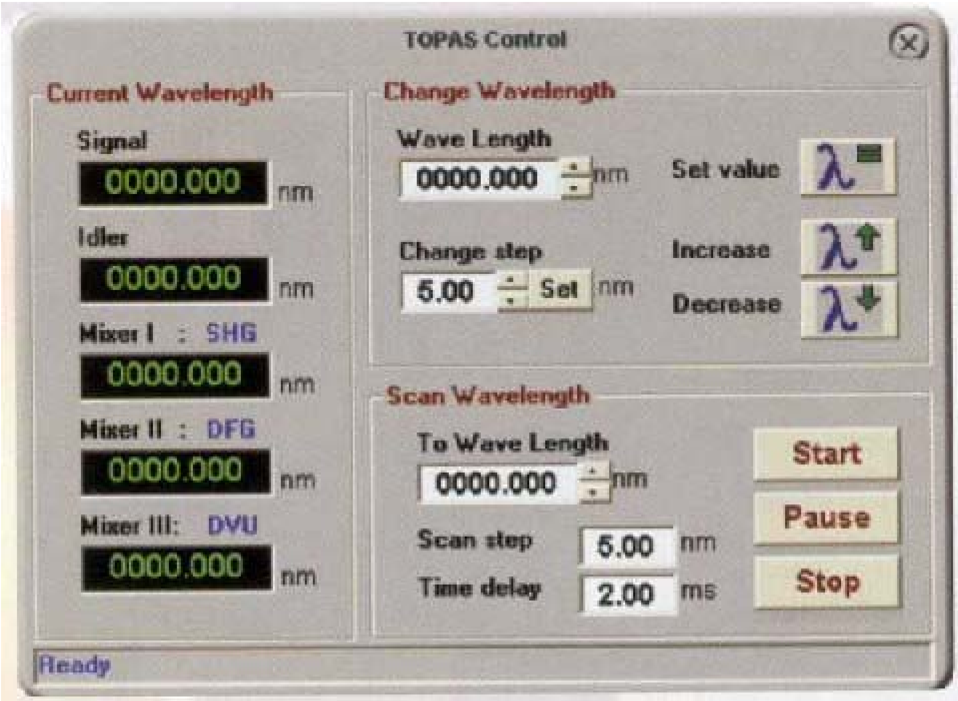

Figure 6.3. Computer controlled wavelength adjustment

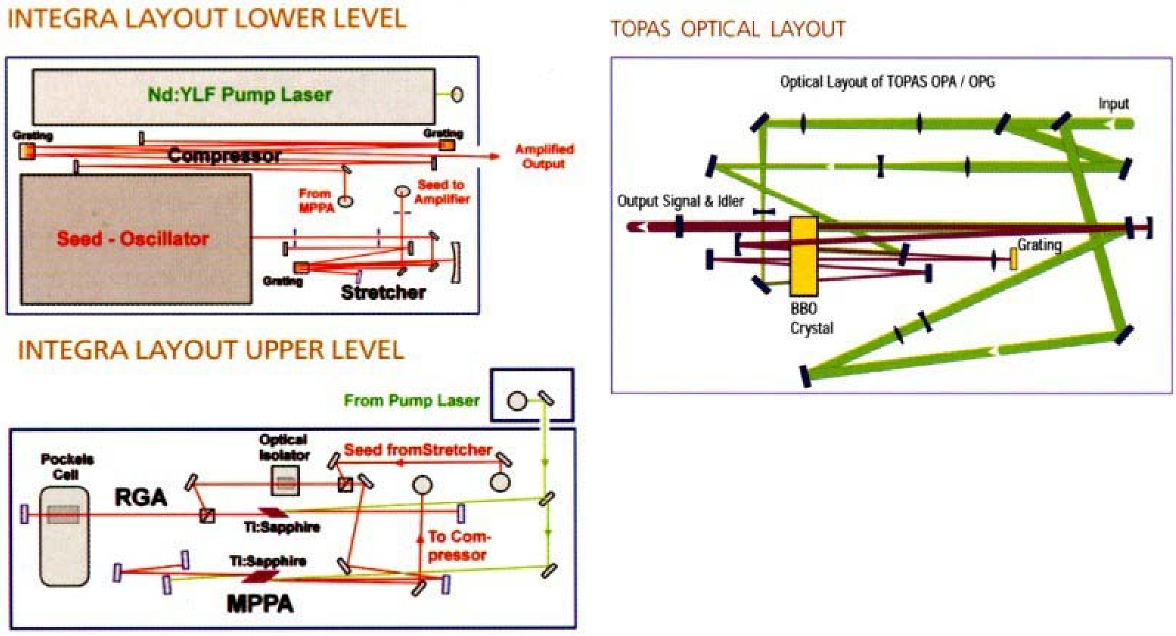

Figure 6.4. Optical pathways in the new system.

7 CONCLUSIONS

7.1 Summary

7.1.1 New techniques have been developed for laser memory mapping. The memory maps have been used to examine previous ion SEE data for the occurrence of MBU's. It was found that MBU's progressively became more common as the ion LET increased. At the highest LET's, numerous very large MBU's were found in the data. These MBU's had been invisible prior to memory mapping, because bits of the same data word are widely spaced in these devices. Without the physical bitmaps, it would be assumed that each error was due to a different event and the device cross-section would be considerably over-estimated.

7.1.2 A new statistical technique has also been applied to the old ion beam data to gain additional insights into the proportions of MBU's. However, the numbers of memory read-cycles during the testing were not large enough for the statistical results to be definitive.

7.1.3 Depth-wise SEE sensitivity profiling has been performed for two SRAM types using multi-wavelength laser testing. The results indicate funnelling of charge from the substrate, if the ionisation path penetrates deep into the substrate. This may not be evident in ion beam facilities, except for the longest range ions.

7.1.4 MBDA have used the SEREEL facility to investigate SEE in two PWM devices, previously ion beam tested by Saab Ericsson. The results have provided indication of the physical die locations at which various types of SET are generated. This also suggests which functions of the circuitry are being upset, by virtue of proximity to bond wires etc. Interesting delayed onset of latchup was observed at one small location on the UCC1806 device. It was often necessary to deliver multiple pulses before a SET occurred. Furthermore, SET's frequently seemed to occur on rising or falling edges of the output pulses. These things suggest that the SET sensitivity was greater when the state of an output was in the process of switching. Overall the results showed extreme variations of the SET sensitivity both spatially across the chip dies and also in time through the output cycles.

7.1.5 MBDA is in the process of a complete redevelopment of its laser SEE testing facility. The new facility is known as SEREEL2 and it will become operational in the second quarter of 2005. SEREEL2 will have greatly enhanced capabilities and improved performance and reliability relative to the current facility. It is anticipated that it will be the best laser SEE test facility in the world.

7.2 Recommendations

7.2.1 Techniques for laser memory mapping and multi-wavelength SEE sensitivity profiling need to be more fully automated in order to make them convenient techniques for day-to-day use. The new SEREEL2 facility has enhanced and expanded capabilities, which will support the automation of these techniques, so it is recommended that further work should be undertaken to apply SEREEL2 for these purposes.

7.2.2 The level of variability discovered in the SEE cross-sections across the PWM microchip surfaces and with time during the output pulse cycles requires a very large number of laser pulses in order comprehensively and quantitatively to characterise the SEE behaviour of these devices (or any similar complex IC's). This will require sophisticated triggering on multiple output conditions. It is recommended that this should be developed in further work.

7.2.3 It is recommended that the ratio of the variance to the mean of the number of errors seen during a read-cycle in memory SEE testing should be monitored continuously throughout the test, since it will provide real time diagnostic indications of the quality of the test results and the proportion of MBU's.

7.2.4 It is recommended that consideration be given to the technical requirements for establishing a preferred or designated laser SEE test facility for the use of ESA and ESA sponsored projects. The MBDA SEREEL2 facility is being developed by MBDA in 2005 with the intention of making the facility accessible and user-friendly for other organisations, so this is a natural context in which to consider this issue.

THIS PAGE INTENTIONALLY LEFT BLANK

DISTRIBUTION LIST

Copy Number	Recipient	Post Box
1	Andrew Chugg	FPC 005, Filton
2-5	Reno Harboe-Sørensen	ESTEC, Keplerlaan 1, PO Box 299, 2200 AG Noordwijk ZH, The Netherlands
6	MBDA Documentation Centre	PB 253, Stevenage